A Multi-Technique Perspective for the Calibration of Metal Dispersion and Oxygen Chemisorption on Ag/TiO_2 Supported Adsorbents

by

Zenda Deena Ann Davis

A dissertation submitted to the Graduate Faculty of
Auburn University
in partial fulfillment of the
requirements for the Degree of
Doctor of Philosophy

Auburn, Alabama
August 1, 2015

Keywords: silver, titanium oxide, chemisorption, x-ray photoelectron spectroscopy, adsorbents, crystallite size

Approved by

Bruce J. Tatarchuk, Chair, Professor of Chemical Engineering
W. Robert Ashurst, Associate Professor of Chemical Engineering
Michael J. Bozack, Professor of Physics
Allan E. David, Assistant Professor of Chemical Engineering

Abstract

Absorption studies were performed in an attempt to gain a better understanding of the discrepancies that exist between the previously reported average crystallite sizes for silver titania adsorbents using oxygen chemisorption and XPS. Oxygen chemisorption, the standard technique for determining average particle size and dispersion is predicated on strong assumptions that easily lead to a misrepresentation of surface characteristics. Accounting for the native uptake of nitrated titania surface and using a Ag/O stoichiometric ratio of 2 for the polycrystalline of the silver titania system surface gave a more accurate representation of the particle size and average crystallite sizes. An atom balance versus Intensity balance demonstrates a bimodal particle size distribution is a representation of the sample. A review is given of the present understanding of silver based adsorbents developed by the Center for Microfibrous Materials Manufacturing. A coherent picture has emerged from the synthesis of all the different studies performed.

Acknowledgments

I would like to thank my family, friends, and colleagues whose support and encouragement have been invaluable throughout this experience. You are all my personal giants on whose shoulders I stand. Thank you.

Table of Contents

List of Figures

List of Tables

List of Abbreviations

Acronyms

A_c	Cross-sectional Area
A_m	Cross-sectional area of the active metal surface atom
ASA	Active Surface Area
BE	Binding Energy
BET	Brunaur-Emmett-Teller
EDS	Energy Dispersive Spectroscopy
EM	Electron Microscopy
EO	Ethylene Oxide
EPR	Electron Paramagnetic Resonance
ESCA	Electron Spectroscopy Chemical Analysis
FCC	face-centered cubic
FPM	First Principles Model
FWHM	Full Width Half Maximum
HSA	Hemispherical Analyzer
ICP-AES	Inductively Coupled Plasma Atomic Emission Spectroscopy
IMFP	Inelastic Mean Free Path

MM	Molecular Weight
N_A	Avogadro's number
N_m	monolayer uptake
NN	Nearest Neighbor
PO	Propylene Oxide
S/V	Surface-to-Volume
S_A	Surface Area
SEM	Scanning Electron Microscopy
SF	Sensitivity Factor
SMSI	Strong Metal Support Interaction
SPM	Scanning Probe Microscope
TCD	Thermal Conductivity Detector
TEM	Transmission Electron Microscopy
TPD	Temperature Programmed Desorption
TPRS	Temperature Programmed Reaction Spectroscopy
TPR	Temperature Programmed Reduction
UHV	Ultra-High Vacuum
XPS	X-ray Photoelectron Spectroscopy
XRD	X-ray Diffraction
X_i	Mole fraction of i

English letter symbols

d	particle dimension
f	particle shape factor
I	Intensity
L	percentage metal loading
m	metal
S	adsorption stoichiometry
s	support

Greek letter symbols

λ	inelastic mean free path; wavelength
ϕ	work function; angular frequency
ρ	density
σ	cross-section; specific surface area

Units

G	Gauss
ppm	parts per million
$ppmw$	parts per million weight
eV	electron volts eV

Definitions

Agglomeration:	The gathering of smaller crystallites into larger particles.
Experimental:	When used in tables mean experimental results.
Crystallite:	A small single crystal. Crystallites are constituents of particles.
Interatomic spacing:	The distance between the nuclei of atoms in a material
Mono-dispersed:	The distribution of a quantity for example, atoms in such a way that they are separated from each other i.e., not touching.
Monolayer:	A singly packed layer of atoms or crystallites.
Nucleate:	To aggregate as a result of the combination smaller crystallites into larger particles.
Particles:	A general term for small object of any size. Particles can be formed from one or more crystallites. In this work, particles correspond to the active phases rather than the support.
Sinter:	To form larger particles or masses by heating, by pressure or both.

Chapter 1

Introduction

Silver supported on titania adsorbents exhibit activities and selectivities for several important industrial applications. One such application is the liquid phase desulfurization of complex fuels [2]. Ambient temperature and pressure desulfurization of liquid transportation fuels offers great advantages when compared to higher temperature and pressure desulfurization. However, the benefits of lower energy and simplicity are often diminished by low capacity for sulfur removal. Ag/TiO_2 adsorbents overcome the obstacle of low capacity usually encountered in the process of desulfurization, while at the same time offering other crucial advantages. These advantages include: good regeneration characteristics, no toxicity, and selective adsorption of refractory aromatic sulfur compounds. Much research has been performed in the development of Ag/TiO_2 sorbents, however, more insight is needed to gain a thorough understanding of the surface structure, adsorbates, and the bonding interactions of the adsorbent system.

At 4 wt% loading, Ag/TiO_2 has been shown to effectively remove sulfur containing heterocyclic compounds from fuels such as JP5, JP8, and Nato F-76. X-ray Photoelectron Spectroscopy (XPS) elemental analysis showed the composition as Ag, Ti, O, and spurious C as expected. The energies of Auger $M_4N_{45}N_{45}$ and XPS $3d_{5/2}$ lines were used to calculate the Auger parameter α for Ag, which indicated that silver is present mainly as Ag^{+1}. This finding was also independently confirmed by the Electron Paramagnetic Resonance (EPR) Spectroscopy. The majority of Ag in the Ag/TiO_2 sorbent was diamagnetic Ag^{+1}, with minor concentrations ($\sim 0.1\%$ of total) as paramagnetic Ag^{+2} [3]. The titanium was present mainly as diamagnetic Ti^{4+}. Further success has been achieved in determining the active

metal dispersion; however, there is some discrepancy regarding the reported mean particle size [4, 5].

Particle size and dispersion are required for a fundamental understanding of the adsorbent system. Adsorption properties change with the dispersion and particle size. Ag/TiO_2 adsorption properties can be correlated to the change in their chemical environment. Specifically, the defected support and the bonding of isolated silver atoms. In an effort to characterize the dimensions of the silver particle; oxygen chemisorption, XRD, XPS, and TEM were used to determine the particle sizes in the Ag/TiO_2 adsorbents. There was a disparity in the results reported among the techniques. Adsorption techniques are sensitive to all crystalline surfaces, where as very small Ag particles will not be detected by XRD and TEM. X-ray diffraction studies indicated particles were less than 5 nm in diameter. Oxygen chemisorption resulted in an over estimation of particle size. These techniques are limited by the fact that they are not a three dimensional evaluation of the particle. However, information received from adsorption techniques is critical in developing an understanding of the nature of active sites. Thus, to fully utilized this technique it is necessary to delineate the interaction of oxygen and Ag crystallites on the TiO_2 support.

In this work, surface studies are proposed to clarify the discrepancies that exist between oxygen chemisorption and XPS. XPS experiments will be used to calibrate oxygen adsorption on silver surfaces. Supporting techniques will be used to complement data regarding the chemical interaction of oxygen on isolated silver supported on TiO_2. The underlying assumptions of oxygen chemisorption will be investigated. Specific studies targeting O_2 monolayer suppression on TiO_2, stoichiometric ratio of Ag to O and the effect of reduction temperature are suggested.

The interaction of oxygen with silver has been studied for a long time. Particularly, because of its use as a oxidation catalyst in important industrial reactions. Reactions not previously mentioned include, epoxidation of ethylene and propylene, oxidation of methane and partial oxidation of methanol formaldehyde. In the literature, oxygen interaction with silver

surfaces is focused on a particular crystal plane. The relevance of those studies maybe limited with respect to multi plane silver surfaces. In this study, investigations were performed on practical silver catalysts with polycrystalline surfaces for industrial catalyst development.

Chapter 2

Literature Review

Sulfur removal from liquid fuels is an important process in the reforming of fuels. Sulfur compounds are unwanted products that need to be removed due to deleterious effects on the environment. Adverse effects are noted in the deterioration of air quality and the sulfur intolerance of specialized equipment such as, catalytic converters, fuel cell electrodes, etc. Although conventional hydro-processing has been effective in reducing sulfur levels, the removal of residual sulfur is inefficient and expensive. The process of removing residual sulfur is energy intensive and is a high consumer of hydrogen. Due to the high cost of hydro-treating, alternative technologies such as adsorptive desulfurization (ADS) have been explored for clean fuel refining. The use of adsorption materials is a more economical and environmentally friendly solution with regards to the challenges presented in removing sulfur from crude with heavy sulfur content. Many adsorptive material that aide in the removal of organic sulfur compounds have been investigated [6–13].

The development of adsorbents with high sulfur capacity, high selectivity and multi-cycle regenerability is needed for advancement. High sorption capacity (g of S per g of sorbent) is needed to remove as much sulfur as possible from a large volume of fuel in a single hydrocarbon stream pass. Selectivity is required to target specific compounds, particularly sulfur containing heterocyclic compounds such as thiophenes derivates and their alkylated derivatives that are difficult to chemically reform [14, 15]. It is also integral that the absorbents be able to resist chemical changes that causes deactivation and has multi-cycle retention properties to achieve competitive and economical sulfur removal. Ambient temperature and pressure ADS of liquid fuels offers great advantages when compared to

higher temperature and higher pressure HDS. The primary advantages being reduction in energy usage, capital and operating costs.

Different materials have been researched for use in adsorptive sulfur removal. The majority of which involves the use of transition metals on high surface area supports such as activated carbon, alumina, silica and titania, etc. [10, 11, 16–22]. The use of zeolites and ion-exchange zeolites as support structures have also been investigated [7, 23–27]. An adsorbent that has been of some use is silver-titania adsorbents [2, 22]. Ag/TiO_2 adsorbents utility involve simple and cost effective preparation, no hydro-processing, ambient operating conditions and multi-cycle regeneration. Also, of paramount significance is its unique properties to selectively adsorb polycyclic aromatic sulfur heterocycles (PASHs) compounds, for example, dimethyl substituted compounds during a single stream pass down to ppm or sometimes ppb levels [22, 28].

Ag/TiO_2 has been characterized using a number of different techniques. These experimental techniques namely, XPS, TPR, EPR, EM, and OC have focused on elucidating the surface properties of the adsorbent [3, 22, 28, 29]. Particle size and dispersion are two crucial parameters to the activity and selectivity of such systems. The four techniques that were employed to study particle size and dispersion were XRD, XPS, TEM, OC. Different techniques have a certain number of disagreements. These disagreements may be due to the sample perspectives, different conditions in different samples, and the assumptions associated with each technique.

X-ray diffraction XRD, is a non-destructive analytical technique which is used to derive information about the crystal structure, chemical composition, and physical properties of materials. With regards to particle size and dispersion, XRD does not give information about dispersion, however a volume weighted average particle size can be derived. There are two main drawbacks of XRD particle size determination. Firstly, the average particle size is volume weighted instead of a more appropriate surface weighted average and secondly, the lower detection limit is reported to be $\lesssim 5$ nm [30–32]. When the irradiated volume is

too small, a sharp diffraction maximum does not build resulting in a diffraction broadened pattern. Thus making this technique inapplicable to particle size below 5nm. An advantage of XRD is that it elemental presence, however, it does not differentiate between oxidation states.

EM can yield information on the topography, morphology, composition, particle size, and crystallography of a given sample. There are several forms of EM available. In this work, only transmission electron microscope (TEM) was used. In TEM, information is projected in two-dimensional image from the interaction of the electron beam with matter encountered. Detection is dependent on the existence of sufficient contrast between the particle and the support.

TEM is a projected area, perimeter weighted average of size distribution. The main advantages of TEM are that it is a straightforward technique and the particles can be viewed from the images created. TEM is very prone to contrast issues; care must be taken during interpretation regarding the possible sources of contrast. Ideally, contrast should be as a result of the attenuation of electrons on the surface of the given sample but, there is also contrast due to diffraction and interference which lead to misinterpretation [33, 34]. It is difficult to contrast supported catalyst material, thus it is not a good technique for particle size determination of supported catalysts. Other disadvantages are that it is destructive, difficult and tedious to prepare; extremely thin sections of specimens, typically about 100 nm are needed. Several samples must be examined with a large number of particles to produce a accurate quantitative representation of the sample.

Gaseous chemisorption, the most extensively used means of determining average particle size and surface dispersion. Of all the techniques discussed, chemisorption gives the most descriptive average weight with regards to the surface area, however the accuracy of the techniques depends on underlying assumptions based on specific characteristics.

Table 2.1: Surface properties of Ag/TiO_2 sorbents with different silver loadings

Ag Loading (wt%)	BET Surface Area (m^2/g)	Pore Volume (ml/g)	Active Metal Surface Area (m^2/g)	Average Crystal Size (nm)	Dispersion %
4.00	114.2	0.2740	6.69	3.4	34.44
8.00	89.33	0.2303	10.7	4.1	28.66
12.00	79.22	0.2115	12.05	5.3	22.35
20.00	57.92	0.1331	14.31	6.9	17.04

Table 2.2: Comparison of experimental techniques

Experimental Techniques	Information Received							
	Visible Species				Particle	Average	Dispersion	Composition
	Ag^x	Ag^0	Ag^{1+}	Ag^{2+}	Size	Weight		
XRD	yes	no	no	no	$\gtrsim$ 5 nm	volume	no	yes
TEM	no	no	no	no	yes	number	no	no
OC	no	no; metal	no	no	yes	surface	yes	no
XPS	yes	yes	yes	yes	yes	near surface	yes	yes

Monolayer formation criteria — a monolayer of chemisorbing atoms (surface atoms exposed) per number of total atoms is assumed to be directly proportional to the specific uptake. Oxygen has been shown to be the adsorbate that most accurately predicts the particle size dimensions of silver, the use of hydrogen and carbon dioxide as probe gases do not result in accurate determination [35–37].

Stoichiometric ratio — Reliable background information regarding the stoichiometric ratio necessary. There is known variation in the stoichiometry ratio of Ag : O (the number of sites per chemisorbed oxygen atom) at the adsorption surface [37]. Although $Ag_{(S)} : O \simeq 1$ appears to be the best value as reported in the literature [38–40] other stoichiometric possibilities have been reported [38]. Other variation in stoichiometry may be due to the hypothesis that the gas molecule to metal stoichiometry is dependent on metal particle size. Thus, if particle there is a significant deviation in particle size, the stoichiometric ratio will be variable.

Absorption selectivity — Gas is adsorbed on the surface and not absorbed internally by the metal and isolated atoms do not adsorb oxygen. Other discrepancies lie in the formation of a complex oxygen adlayer on silver [41, 42]. Other complexities arise when there are carbonaceous contaminants which have an effect on the sorption behavior of oxygen due to possibility of subsurface oxidation of silver [38]. Other problems that may arise include, multiple adsorption of oxygen molecule on metal surface atoms, internal absorption, incomplete adsorption of the oxygen molecules by the metal particles, and non-metallic silver particles.

Particle Characteristics — In chemisorption, unimodal particle size, crystallite formation and geometry are assumed. Variation in any of these characteristics will produce slightly different average dimensions. Factors that result in exaggerated crystallite size would be adsorption by the support, in this case, titania, subsurface adsorption, multiple adsorption of gas molecule on metal surface atoms and under estimation of the stoichiometric ratio

[43]. Lower crystallite size would result from over estimation of the stoichiometric ratio and inability of absorbate gas to selectively chemisorb a monolayer.

XPS is a non-destructive, surface analysis technique that gives a near-surface weighted measurement of the average particle dimension. Like chemisorption, XPS is a well established as a technique for studying surface atom dispersion and particle size of metal on supported systems [44–53], however, in comparison it is less often used to acquired particle size dimension [31, 54–58]. In XPS, the particle size is determined without extensive pretreatment in comparison to the other techniques. This is important as pretreatment may alter the state of the particle or crystallite in question. XPS is the only technique of these which use enable the characterization of all elements with the exception of hydrogen. Also, a marked distinction from chemisorption is its applicability to metal and non metals, reducible and irreducible phases. Atoms on the surface and subsurface will be seen irrespective if oxidation state. The basic assumptions underlying XPS are:

- The number of electrons recorded is proportional to the number of atoms in a given state
- Variation in the chemical environment does not appreciably affect the overall ejected photoelectrons
- Mono-dispersion of surface atoms

Despite its own inherent perspectives, this technique is actually able to simultaneously account for oxidation, degree of dispersion, and nucleation/growth and not either or. XPS observes the surface from the same perspective as surface and heterocyclic interactions not just visible versus invisible species as observed by different techniques.

2.1 Surface Chemistry of Silver-Titania Adsorbents

2.1.1 Adsorbent Preparation

Silver-titania adsorbents were made from 3.2 mm TiO_2 pellets [St. Gobain Norpro: Type ST61120]. The pellets were crushed, sieved and dried in a convection oven for at least 6 hours at 110 °C. Ag was dispersed on the support in the form of $AgNO_3$ solution [Alfa Aesar Co. 99.9 % purity] via incipient wetness impregnation to maintain 90 % of the pore volume of the TiO_2. The concentration of the $AgNO_3$ solution was varied according to the required load. The sample was subsequently dried at 110°C for 6 hours followed by calcination in air at 400°C for 2 hours.

2.1.2 Surface Properties

Table 2.3: Surface Properties of Ag/TiO_2 Sorbent.

Ag Loading (wt%)	BET surface area (m^2/g)	Pore Volume (ml/g)	Active Ag surface area (m^2/g)	Average crystal size (nm)	Dispersion (%)
0.00	153	0.46	–	–	–
4.00	114	0.27	6.7	3.4	34.4
8.00	89	0.23	10.7	4.1	28.7
12.00	79	0.21	12.1	5.3	22.4
20.00	58	0.13	14.3	6.9	17.0

Table 2.3 states the surface properties of Ag/TiO_2 sorbent used in this study. This data was previously published by Nair [22]. At 0 – 20 wt % loading Ag is present in the oxide phase. EPR and TPR analyses indicated that Ag is present in its oxide state as Ag^{1+} with minor concentrations present as Ag^{2+} [28]. TPR showed that the majority of Ag was present

in the oxide phase at higher loading (greater than 4 wt%). Oxygen chemisorption was used to determine the average crystallite size of the silver particles on the surface.

2.2 Silver Crystal Structure

Ag has a face centered cubic (FCC) crystallographic structure with 4 atoms per unit cell – the Ag unit cell contributes 1/2 of an atom on each of its 6 faces to each unit, and 1/8 th of an atom at each of its 8 corners totaling 4 atoms. In the bulk, each atom has 12 nearest neighbors thus a coordination number of 12. The Ag (111) structure exposes a surface atomic arrangement of 3 fold symmetry which appears to be hexagonal. Fig 2.1 depicts the hexagonal packing of the surface atoms, which is the most efficient (closely packed) manner of atomic arrangement. The coordination number of the surface layer on the fcc (111) surface is 9; each atom has 6 nearest neighbors in the 1st layer and 3 in the layer below, totaling 9 atoms.

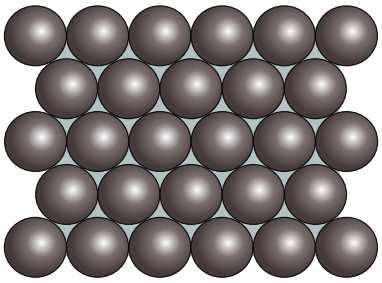

Figure 2.1: Birds eye view of an fcc structure of (111) plane

The density of atoms in Ag FCC (111) crystal plane is calculated from the lattice parameter, a. Since two corner atoms and and a central atom make up the length of the side diagonal of the FCC (see Figure 2.2), the lattice parameter is given by:

$$a^2 + a^2 = (4R)^2$$

$$a = \frac{4}{\sqrt{2}} = 2R\sqrt{2}$$

$$a = 4.08 \text{ Å}$$

The atomic density per cubic cm^3 of Ag(111) surface is:

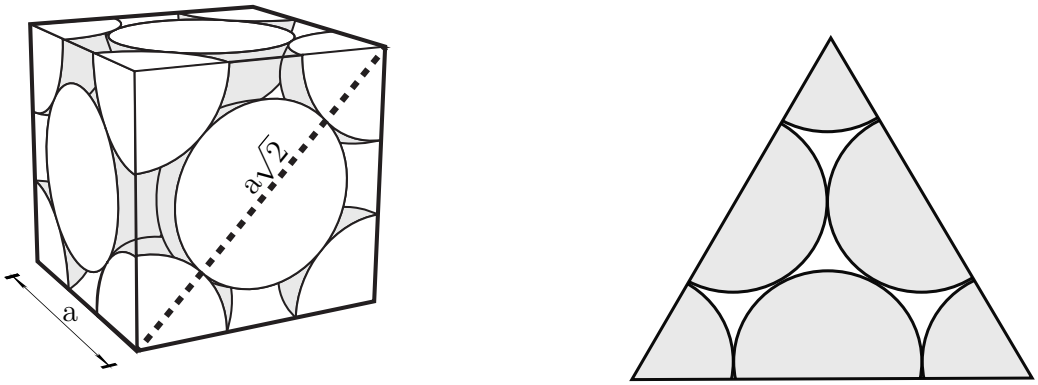

(a) 3d view of a unit cell **(b)** cross-sectional view

Figure 2.2: FCC structure of (111) plane

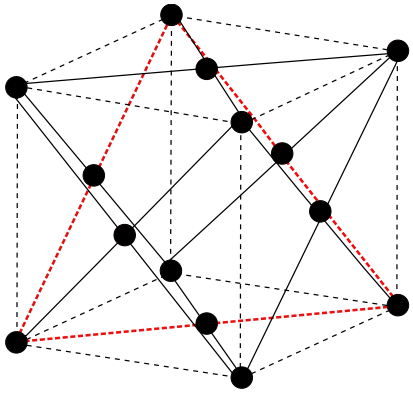

Figure 2.3: FCC (111) plane

$$\begin{aligned}\text{Ag atomic density} = \frac{\#\text{ of atoms per unit cell}}{\text{Volume of unit cell}} &= \frac{4}{a^3} \\ &= \frac{4}{(4.08 \times 10^{-10}\ \text{m})^3} \\ &= 5.88 \times 10^{28}\ \text{atoms/m}^3\end{aligned}$$

The number of surface atoms is dependent on the surface structure. Considering the crystallographic surface heterogeneity of polycrystalline surfaces for dispersed metals, the

usual approximation is to assume that such surfaces are formed from equal proportions of the main lox index planes [36]. Using this assumption, equal portions of the (100), (110) and (111) planes was used to estimate the polycrystalline planar concentration.

Density of atoms in Ag(111) crystal plane

$$\text{No. of atoms contained in Ag (111) plane} = \left(\frac{1}{6} \times 3 \text{ corners}\right) + \left(\frac{1}{2} \times 3 \text{ sides}\right) \text{atoms}$$

$$= 2 \text{ atoms}$$

$$\text{Area of Ag (111) plane} = \frac{a^2\sqrt{3}}{2}$$

$$\text{Surface density of atoms in Ag (111) crystal plane} = \frac{2}{\frac{a^2\sqrt{3}}{2}} = \frac{4}{a^2\sqrt{3}}$$

$$= \frac{4}{(4.08 \times 10^{-8})^2 \times \sqrt{3}}$$

$$= 1.38 \times 10^{19} \text{ atoms/m}^2$$

Density of atoms in Ag(110) crystal plane

$$\text{No. of atoms contained in Ag (110) plane} = \left(\frac{1}{4} \times 4 \text{ corners}\right) + \left(\frac{1}{2} \times 2 \text{ diagonal center}\right) \text{atoms}$$

$$= 2 \text{ atoms}$$

$$\text{Area of Ag (110) plane} = a^2\sqrt{2}$$

$$\text{Surface density of atoms in Ag (110) crystal plane} = \frac{2}{a^2\sqrt{2}}$$

$$= \frac{2}{(4.08 \times 10^{-10})^2 \times \sqrt{2}}$$

$$= 0.85 \times 10^{19} \text{ atoms/m}^2$$

Density of atoms in Ag(100) crystal plane

$$\text{No. of atoms contained in Ag (100) plane} = \left(\frac{1}{4} \times 4 \text{ corners}\right) + (1 \text{ center}) \text{ atoms}$$

$$= 2 \text{ atoms}$$

$$\text{Area of Ag (100) plane} = a^2$$

$$\text{Surface density of atoms in Ag (100) crystal plane} = \frac{2}{a^2}$$

$$= \frac{2}{(4.08 \times 10^{-10})^2}$$

$$= 1.20 \times 10^{19} \text{ atoms/m}^2$$

Generally, in heterogeneous catalysis, only a monolayer (ML) of a chemisorbed species is adsorbed to the active sites. Assuming equal proportions of the Ag low index planes the number of Ag atoms in a ML is estimated to be 1.14×10^{15} atoms/cm^2.

2.3 Determination of Particle Size

2.3.1 Chemisorption

Gas phase chemisorption is the most extensively used technique for determining particle size and surface atom dispersion of supported metal catalysts in heterogeneous systems [32, 35, 37, 38, 43, 60–64]. In this technique, a monolayer of chemisorbing atoms (surface atoms exposed) per number of total atoms is assumed to be directly proportional to the specific uptake. Oxygen has been shown to be the adsorbate that most accurately predicts the crystallite size dimensions of silver, the use of hydrogen and carbon dioxide as probe gases do not result in accurate determination of silver particle size [35–37]. The underlying theoretical assumptions of chemisorption are:

- Monolayer formation criteria - a monolayer is chemisorbed

- Stoichiometric ratio
- Adsorption selectivity
- Gas is adsorbed on the surface and not absorbed internally by the metal
- Unimodal particle size
- Crystallite formation
- Crystallite geometry
- Isolated atoms do not adsorb oxygen

Perspectives

Chemisorption is a simple, well-established surface weighted means of calculating the average particle diameter. Of all the techniques considered in this chapter, it is the most readily available techniques. Chemisorption is a surface area weighted average distribution of the vital size. The accuracy of the techniques relies on background information, namely, the correct stoichiometric ratio, and the ability of a absorbate gas to selectively chemisorb on the active metal provided that there is constant gas uptake on the support when the metal is present or absent. For the Ag/TiO_2 adsorbent, there may be problems due to the variation in the stoichiometry ratio of Ag : O (the number of sites per chemisorbed oxygen atom) at the adsorption surface [37]. Although $Ag_{(S)} : O \simeq 1$ appears to be the best value as reported in the literature [38–40] other stoichiometries possibilities have been reported [38]. Differences in stoichiometries may be due to the hypothesis that the gas molecule to metal stoichiometry is dependent on metal particle size. Other discrepancies lie in the fact that the oxygen adlayer on silver has been reported to be complex [41, 42]. Complexities arise to carbonaceous contaminants which have an effect on the sorption behavior of oxygen due to possibility of subsurface oxidation of silver [38].

In chemisorption, there is size variation depending on the crystallite geometry assumed, for example, spherical and cubic geometries will produce slightly different average dimensions. Other problems that may arise include, multiple adsorption of oxygen molecule on metal surface atoms, internal absorption, incomplete adsorption of the oxygen molecules by the metal particles, and non-metallic silver particles. Of these problems, explanations for exaggerated crystallite size would be adsorption by titania support – subsurface adsorption and multiple adsorption of gas molecule on metal surface atoms – under estimation of the stoichiometric ratio [43]. Lower crystallite size would result from over estimation of the stoichiometric ratio and inability of absorbate gas to selectively chemisorb a monolayer.

2.3.2 X-ray Photoelectron Spectroscopy

XPS is based on the detection of photoelectrons from a sample irradiated by an X-ray source. The detected photoelectrons are recorded in a energy spectrum. This energy spectrum is analyzed to produce a wealth of chemical information about the sample under investigation. XPS is sensitive for trace amounts of all elements with the exception of hydrogen. Quantitative information is received only from the top 10 nm of the surface thus, XPS is defined as a surface analysis technique. Like chemisorption, XPS is well established as a technique for studying surface atom dispersion and particle size of metal on supported systems [44–53], however, in comparison it is less often used to acquire particle size dimension [31, 54–58].

The basic assumptions underlying XPS are:

- The number of electrons recorded is proportional to the number of atoms in a given state
- Variation in the chemical environment does not appreciably affect the overall ejected photoelectrons
- Mono-dispersion of surface atoms

Perspectives

XPS is a non-destructive, surface analysis technique that gives a near- surface weighted measurement of the average particle dimension. Although there is general agreement that XPS offers a surface weighted characterization of particle dimension, Fung [31] postulated that XPS also adds a volume aspect such that it gives an account of the particle dimension based between the surface and volume average size. In XPS, the particle size is determined without extensive pretreatment with regards to other techniques. This is important as pretreatment may alter the state of the particle or crystallite in question.

XPS is broadly applicable – all elements can be observed in XPS with the exception of hydrogen. Also, unlike chemisorption, XPS is applicable to metal and metal oxides (reducible and irreducible phases). XPS offers good chemical resolution and depth resolution. The shortcomings of the past regarding poor spatial resolution and detection limit [65] have been improved upon in recent years [66–68].

2.3.3 X-ray Diffraction

X-ray diffraction XRD, is a non-destructive analytical technique which is used to derive information about the crystal structure, chemical composition, and physical properties of materials. In XRD, the scattered intensity of X-ray radiation is used to produce photon energy spectra as a function of the incident and scattered angle, polarization, and wavelength on a given sample. The spectra produced are characteristics of the composition of the sample. The scattered monochromatic X-rays are the result of constructive interference by the atoms in the crystal plane. Crystalline material produce diffraction maxima according to the Bragg equation:

$$n\lambda = 2dsin\theta \tag{2.1}$$

where n is an integer, λ is the wavelength of incident wave, d is the spacing between the planes in the atomic lattice, and θ is the angle between the incident ray and the scattering

planes. The average crystallite size is determined by X-ray broadening [69, 70] by the Scherrer expression:

$$D = \frac{k\lambda}{\beta cos\theta} \tag{2.2}$$

where D is the mean diameter, β is the pure X-ray diffraction broadening and k is a constant ≈ 1. k and β are constants dependent on the crystallite shape.

Perspectives

XRD is a non-destructive, volume weighted means of determining crystallite size. The major weakness of this technique lies in the determination of small crystallites. If the irradiated volume is too small for a sharp diffraction maximum to build up, the resulting diffraction pattern is broadened [70]. From the literature, the lower detection limit is reported to be $\lesssim$ 5 nm [30–32]. However, when a synchrotron radiation source is used, platinum particles as small as 1.5 nm have been estimated [72]. This is a result of a better signal to noise ratio produced using the high intensity radiation.

The agreement between X-ray line broadening (XRD) and gaseous chemisorption is good when particles are greater than > 5 nm and < 100 nm [35]. XRD did not provide conclusive measurements when applied in the crystallite size determination of Ag/TiO_2 adsorbents. The lack of signal suggested that the crystallite was below the detection limit of the XRD $\lessapprox$ 5 nm. This is a result of X-ray broadening of the diffraction beam produced from very small crystals at angle close to the Bragg angle [70, 71]. Strong diffraction beam pattern form from bigger crystals than smaller crystal. Since, the instrumental peak width was much larger than the broadening due to crystallite size, the crystallite size could not be determined. A silver peak was detected at the 20 wt% loading. Due to its small size and broad width, however, a size dimension could not be reliably determined.

2.3.4 Electron Microscopy

Electron microscopy EM, is the near atomic scale microscopic examination of objects, through the use of highly energetic electrons (produced form a highly focused X-ray beam). EM can yield information on the topography, morphology, composition, and crystallography of a given sample. There are several forms of EM available. In this work, only transmission electron microscope (TEM) will be employed. In TEM, information is projected in two-dimensional image from the interaction of the electron beam with matter encountered. Detection is dependent on the existence of sufficient contrast between the particle and the support.

Perspectives

EM is a projected area, perimeter weighted average of size distribution. The main advantages of TEM are that it is a straightforward technique and the particles can be viewed from the images created. However, care must be taken during interpretation regarding the possible sources of contrast. Ideally, contrast should be as a result of the attenuation of electrons on the surface of the given sample but, there is also contrast due to diffraction and interference which lead to misinterpretation [33, 34]. TEM is very prone to contrast issues. It is difficult to contrast supported catalyst material, thus it is not a good technique for particle size determination of supported catalysts. Other disadvantages are that it is destructive and difficult to prepare; extremely thin sections of specimens, typically about 100 nm are needed. Several samples must be examined with a large number of particles to produce a accurate quantitative representation of the sample.

The application of the TEM using the diffraction contrast method proved to be fruitless in the determination of particle size on the Ag/TiO_2. Information on particles size was not discernible from the bright and dark field images produced [73].

2.4 XPS Analysis

This section contains background experimental information from 'A Multi-Technique Comparative Evaluation of Ag Dispersion on Polycrystalline Titania'. This information is necessary to provide a full understanding of the motivation for the subsequent studies performed.

The XPS survey spectra revealed significant compositions of the following elements: Ag, Ti, O, C. Nitrogen from the $AgNO_3$ precursor was not detected in the samples. The XPS spectra in Figure 2.4 show the experimental data of the Ag 3d doublets of Ag/TiO_2 adsorbents ranging in silver loading from 1 wt% - 20 wt%.

At the 1 wt% loading the Ag signal intensity was below the detection limit of the XPS; a weak signal was detected at the 2 wt% loading; the Ag peak intensity increased in prominence up to 20 wt% loading. The spectra showed a slight shift toward a lower binding energy (BE) of the Ag 3d doublet peaks at the 12 wt% loading and 20 wt% loading. A shift in the binding energy is a result of a change in the chemical bonding of the atoms in a solid. Several factors such as valence electron density, lattice potential, work function, and atomic relaxation energy are reported to influence a shift in BE [74, 75]. If ionic charge or oxidation state were the only factors to be considered, then it could be concluded that Ag was reduced. However, the anomalous nature of the BE of Ag oxides compared to that of Ag metal is such that there is a negative shift in BE from Ag^0 to $Ag^{1+,\ 2+}$ [76, 77]. Normally in the literature, most metal to metal oxides systems exhibit positive binding energy shifts as the metal is oxidized. Positive shifts are typically the result of screening effects which resulting in electronegativity differences. The metal cation has a reduced number of electrons screening the nucleus which typically results in a higher binding energy for the metal oxides than the metal.

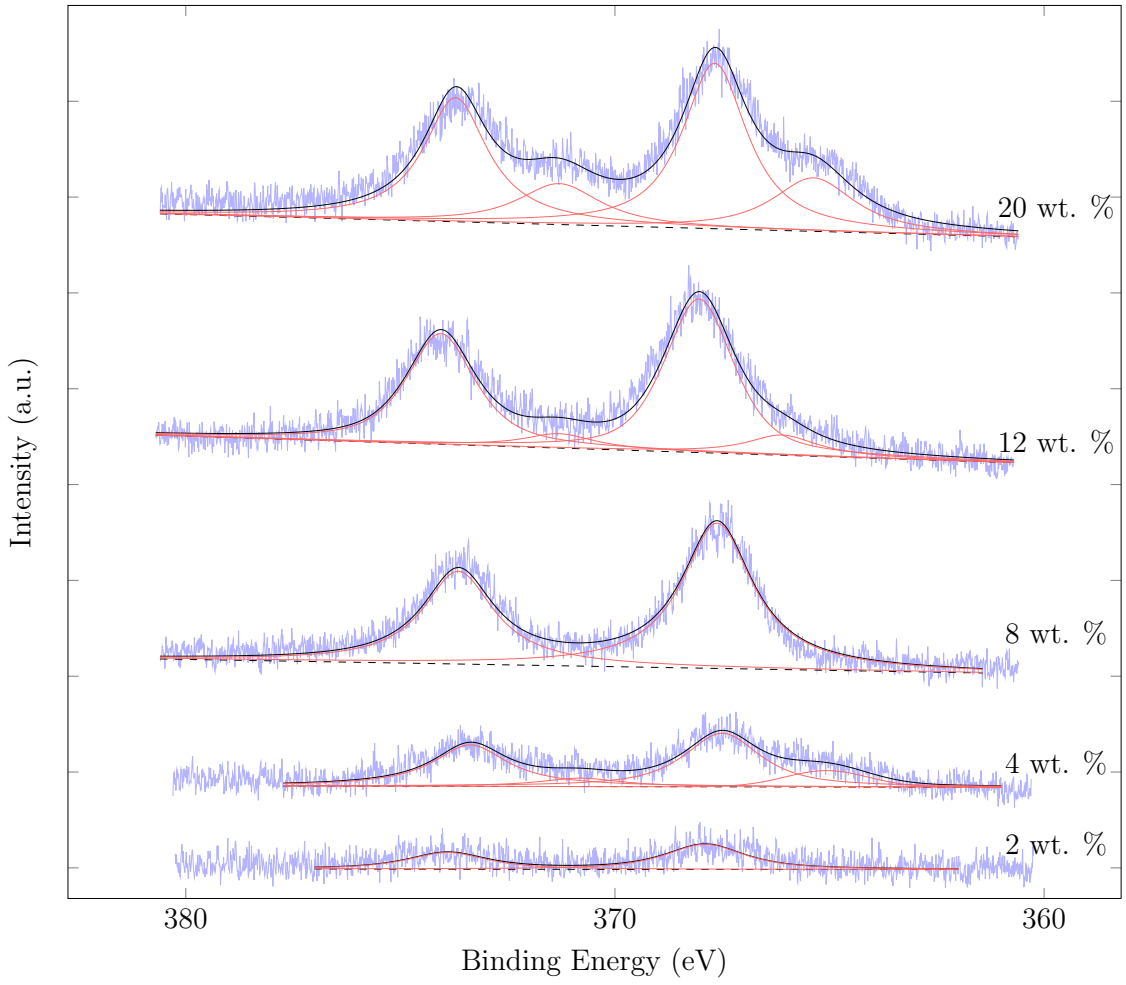

Figure 2.4: Deconvolution of XPS spectra of the Ag/TiO_2 $Ag(3d_{3/2}, 3d_{5/2})$ peaks ranging from 1–20 wt% loading

Table 2.4: FWHM and BE of Ag-3d Peaks

Ag/TiO_2	Binding Energy (eV)							
	Component 1				Component 2			
Loading	$Ag(3d_{3/2})$	FWHM	$Ag(3d_{5/2})$	FWHM	$Ag(3d_{3/2})$	FWHM	$Ag(3d_{5/2})$	FWHM
1 wt%	UD	UD	UD	UD	UD	UD	UD	UD
2 wt%	373.9	2.3	367.9	2.3	UD	UD	UD	UD
4 wt%	373.5	2.1	367.5	2.1	370.8	2.1	365.1	2.1
8 wt%	373.7	2.1	367.6	2.1	UD	UD	UD	UD
12 wt%	374.0	2.0	368.0	2.0	371.3	2.0	365.3	2.0
20 wt%	373.7	1.9	367.7	1.9	371.3	2.3	365.3	2.3

UD - undetectable

† uncertainty ± 0.2 eV

The decomposition of the Ag 3d photoemission spectra is shown in Figure 2.4. Photoelectron lines have a Lorentzian shape corresponding to the lifetime of the core hole that is created; if all the features were ideal a strictly Lorentzian curve would be used. However, a combination of Gaussian-Lorentzian curve was used to account for non-idealities in the system; instrumental factors such as the width of the x-ray line and the analyzer resolution. This mixed curve ratio was employed for the entire analysis. Symmetrical line shapes were used for all elements. Several parameter constraints were employed in consideration of known physical constants of Ag in order to obey the chemistry. These parameters were: the peak symmetry - defined by the d-subshell, a doublet separation of 6.0 $\pm$ 0.2 eV, and the relative intensities for d electrons, 2:3 [75, 78, 79]. A proper background was also necessary to obey the chemistry and physics involved in the system. A blend of the Shirley and linear backgrounds was used to satisfy the 2:3 ratio of the d doublet. The Gaussian-Lorentzian curve ratio, the relative intensity 3d doublet area ratio, and the peak separation were all fixed. The FWHM of the peaks were constrained within a range. The use of the physical constants and constraints should reduce ambiguity, elucidate underlying peaks, and eliminate the introduction of biases that would result in a loss of the contribution of other peaks. The peaks were fitted with a fair degree of certainty because of these physical constants and constraints. Changes in oxidation state of Ag could not be determined due to the slight differences in BE values using the ($3d_{5/2}$) peak binding energies Ag^0 (368.2 eV), Ag^{1+} (367.7 eV), and Ag^{2+} (367.4 eV) [75, 76, 79]. Additionally, this determination was beyond the sensitivity of the non-monochromatic LHS-10 XPS system which had an uncertainty of $\pm$ 0.2 eV.

The prominent shoulders displayed in the 20 wt% loading were attributed to the occurrence of a second doublet component. The Ag silver at the 12 wt% loading showed an anomaly in that the BE of the Ag 3d peak displayed the highest BE of all the sample analyzed. This occurrence was independently verified [80]. The 4, 12 and 20 wt% loading were decomposed into two doublets. The multiple occurrence and growth of the second doublet

suggest that this is not an artifact resulting from system contamination. The second doublet suggests the occurrence of multiple species of Ag_xO_x. Table 2.4 shows the BE and the FWHM values for the components of the XPS Ag 3d spectra. The BE of the silver oxides decrease in the order Ag_m – Ag_2O – AgO while the FWHM increases and the peaks get broader. The first Ag component is assigned to Ag_2O with Ag $3d_{5/2}$ located at 365.6 ± 0.2 eV as is reported in literature (see Table 2.5). The FWHM of this component decreases with increasing weight loading. AgO is reported to have two chemically inequivalent silver atoms with chemical formula $Ag^{I}Ag^{III}O_2$. Ag^{I} has two oxygen atoms and Ag^{III} with four oxygen atoms [76].

Table 2.5: BE of $Ag(3d_{5/2})$ Peak in Ag, Ag_2O, and AgO

Compound	Binding Energy (eV)	Reference
Ag	368.1 ± 0.1	Schön [76]
Ag	368.0	Gaarenstrom [75]
Ag	367.9	Wagner [79]
Ag	367.9 ± 0.2	This work
Ag_2O	367.7 ± 0.2	Schön [76]
Ag_2O	367.6	Gaarenstrom [75]
AgO	367.8	Wagner [79]
AgO	367.4 ± 0.2	Schön [76]
AgO	367.2	Gaarenstrom [75]

Table 2.5 shows the values of the BE of $Ag(3d_{5/2})$ peak in Ag, Ag_2O, and AgO found in literature. Oxygen displays distinctive features which are characteristic to metallic silver and Ag_xO_x compounds; Ag^0 has a peak at 532.2 eV, Ag^{1+} has two peaks at 529.0 eV and 530.4 eV, and Ag^{2+} has two peak at 528.4 eV and 530.3 eV [76]. The major contribution to the oxygen peak is TiO_2 as demonstrated by the mole ratios presented in Table 2.6. This qualifies

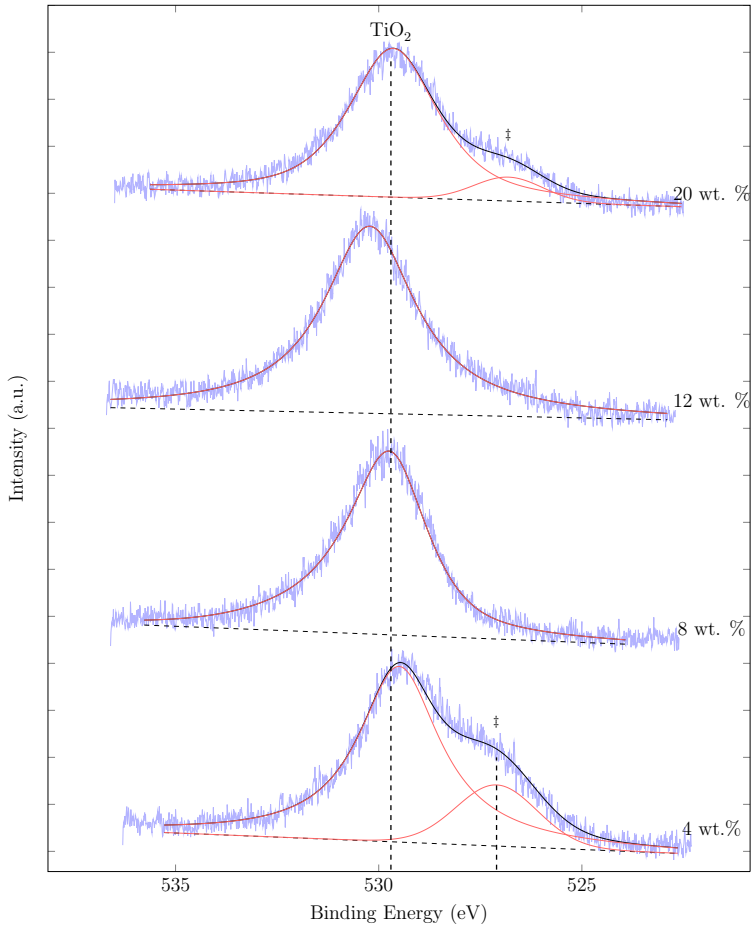

‡ - indicates multiple oxygen species

Figure 2.5: Oxygen 1s spectra of various loading of Ag/TiO_2 adsorbents

the assignment of the peak occurring at approximately 529.5 eV to TiO_2. Additionally, there is most likely a small contribution from Ag_2O and AgO, but that contribution could not be extracted from this data with great fidelity. However, it can be concluded that the oxygen peaks show the presence of multiple species. The change from one component to two component in the oxygen peak could be due to continuously changing oxygen absorbed on Ag_2O to metallic Ag noted in metal-oxygen systems reported in Schön [76]. Previous TPR investigations revealed that Ag is present in its oxide state as Ag^{1+} with minor concentrations present as Ag^{2+} [28].

Atomic Ratios

Atomic ratios derived from the XPS data are listed in Table 2.6. The atomic ratios of TiO_2 are fairly constant for all the weight loadings, except for the 2 wt% loading. This shows that the titania support was not appreciably obscured by the silver deposited. The deviation in the 2 wt% sample can be explained by the increased levels of carbon which suggested carbon contamination. Similarly, the atomic ratios of oxygen are fairly constant across the various loadings, except for the 20 wt% sample where it is hypothesized that reduction took place. The O/Ti ratios did vary at the 2 and 20 wt% loadings. It is believed that deviated occurred at the 2 wt% due to carbon contamination and at 20 wt% as a result of some chemical structural change.

Dispersion

Information regarding the dispersion and particle size of silver particles on titanium oxide support was extracted using the XPS. XPS has been well established as a technique for studying dispersion of metal on supported systems [45–50, 55, 64, 81–85]. 2.6 shows the intensities of the active particles relative to the support versus the mole fraction as detected by the XPS for various loadings of silver particles. The XPS intensity ratio for Ag/TiO_2 increases with additional loadings of silver. There is a linear relationship observed

Table 2.6: Atomic Ratio of Surface Species on Ag/TiO_2 Adsorbent Pellets

	Ag/TiO_2 Loading					
Element	1wt%	2wt%	4wt%	8wt%	12wt%	20wt%
C-1s	0.25	0.31	0.21	0.19	0.19	0.22
O-1s	0.52	0.51	0.53	0.52	0.51	0.46
TiO_2-2p	0.23	0.17	0.23	0.23	0.23	0.22
Ag-3d	UD	0.01	0.03	0.06	0.08	0.10
Theoretical Ag†	0.008	0.015	0.03	0.06	0.09	0.15
Total	1.00	1.00	1.00	1.00	1.00	1.00

‡ - uncertainty $\pm$ 10%

UD - undetectable

† - calculated based on the Ag deposited on specimen.

at lower loadings of less than 0.03 mole fraction (<4 wt%) which suggests that silver is highly dispersed on the titanium oxide support up to a certain critical value. At this critical value, theorized to be between 4 and 5 wt% , increased silver loading deviates from the linear trend and levels off smoothly. This points to the growth of silver particles. Initially, particles are likely to be of uniform distribution and are well dispersed on the surface of the support until they reach a critical loading where the particles begin to grow in size. Similar trends have been observed in the literature [46, 85, 87]. Briggs [46] observed the peak areas of metal catalysts supported on silica versus the wt% metal loading in M/SiO_2 catalyst[1] and Park [85] observed the XPS Cr 2p/Al 2p intensity ratios. This theory is also supported by the fact that sulfur capacity for the Ag/TiO_2 adsorbent increases with weight loading up to a critical value, between 4 and 5 wt% after which increased loading does not increase sulfur capacity [22].

[1]the identity of M was not disclosed

The dashed line in Figure 2.7 and 2.8 exemplifies the trend that would result if the silver-to-titania intensity ratios exhibited a strong linear dependence with loading; however, the experimental values, as indicated by the solid line, did not show this dependence. This dependence was calculated assuming all the silver was atomically dispersed and every atom was accessible (best case scenario). The 2, 4, and 8 wt% Ag/TiO_2 loadings conformed to uniform dispersion. At the 12 wt% the experimental value falls slightly below the calculated values and at 20 wt%, the adsorbent with the highest loading, the value falls significantly below linear dispersion line. It is important to note that high and uniform dispersion is important to gain the greatest access to the active atoms of the adsorbent.

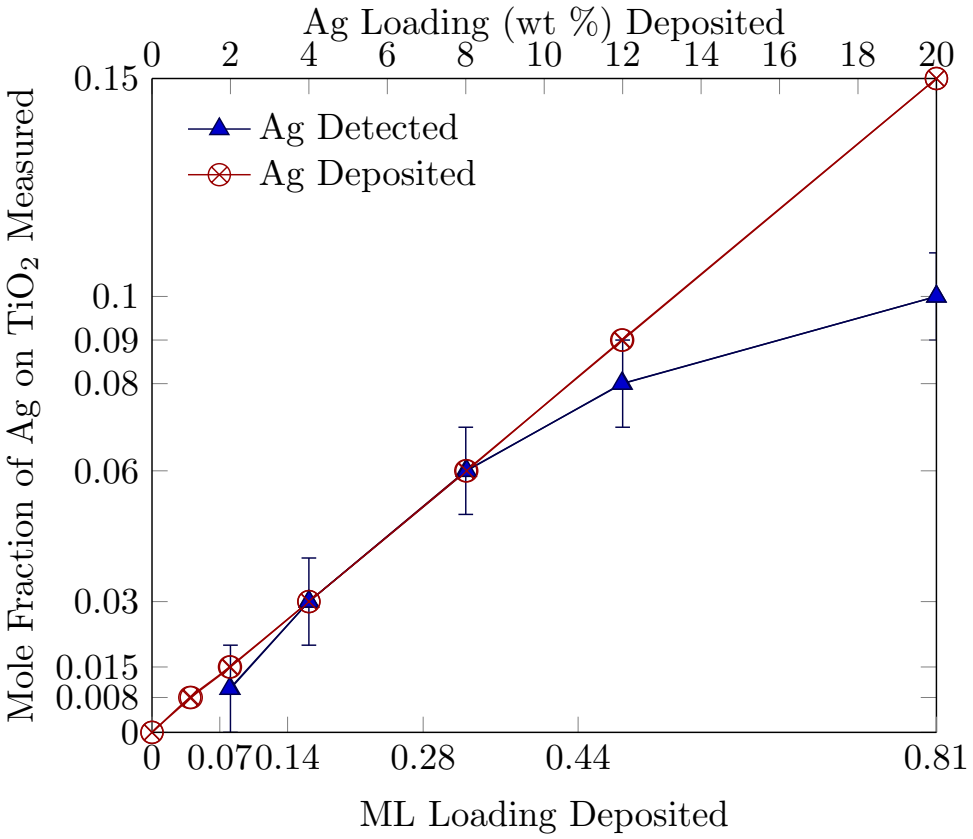

Figure 2.6: Monolayer detected versus moles deposited of Ag

Particle Size

In addition to dispersion, the properties of a catalyst are to a large extent dependent on particle size. However, the atomic size difficult to predict. Difficulties arise in compounds because of nearest neighbors interactions and the resulting perturbation on the electron charge cloud. Despite these difficulties, a best estimation is a useful starting point. If the assumption is made that isolated Ag atoms are all uniformly dispersed on the support, then an estimation can be made to locate the point beyond which the Ag particles begin to increase in size based on a comparison of the experimental I_{Ag}/I_{TiO2} and the calculated I_{Ag}/I_{TiO2} assuming 100% accessibility of Ag atoms.

The data displayed in Figure 2.7 suggests that all the Ag atoms are accessible up to 8 wt% loading after which the crystallites growth occurs. This is signified by the departure from the linear behavior demonstrated from 0 wt% up to 8 wt%. Another linear trend is displayed from 8 wt% to 20 wt% which indicates that the particles form crystallites that are uniform in size and increase in occurrence with increased loading up to 20 wt%. The I_{Ag}/I_{TiO_2} experimental values form 0 – 8 wt% loadings lie on a line which typically indicates uniform dispersion. Since non-linear behavior starts after 8 wt% loading, it was assumed that nucleation occurred beyond this point. Table 2.7 lists the predicted I_{Ag}/I_{TiO_2} values due to particle growth. The predicted values at 12 wt% fell at the lower end of the uncertainty range while at the 20 wt% loading the predicted value was just outside the uncertainty range.

In Figure 2.8 particle growth is assumed to start after 4 wt% loading. The corresponding values are listed in Table 2.8. The predicted I_{Ag}/I_{TiO_2} values are well within the uncertainty range. The results listed in Tables 2.7 and 2.8 indicates that arguably the Ag particle growth could be somewhere between 4 wt% than 8 wt%. However, since the sulfur heterocyclic adsorption selectively has the greatest capacity at about the 4 wt% loading a more confident assertion is that particle growth begins at this point.

Predicted Particle Size

The dimension change of the crystallites were found by equating the particle growth term as seen in Equation 2.3 to the I_{Ag}/I_{TiO_2} experimental values. Particle growth was assumed to begin after 4 wt% loading.

$$I_{Ag} = B_0 \sigma_{Ag} \lambda_{Ag}(\epsilon) N_{Ag} \underbrace{\int_0^t e^{-t/\lambda} \, \mathrm{d}t}_{growth\ term} \tag{2.3}$$

The final dimensions can be calculated by accounting for the initial atomic size plus the growth dimension. One Ag atomic diameter is equivalent to approximately 0.35 nm. If a crystallite at the 8 wt% loading contains 2 atoms on an edge of a cube then the total number of atoms contained would be 8 atoms. The subsequent size at 8 – 20 wt% loadings are listed in Table 2.8

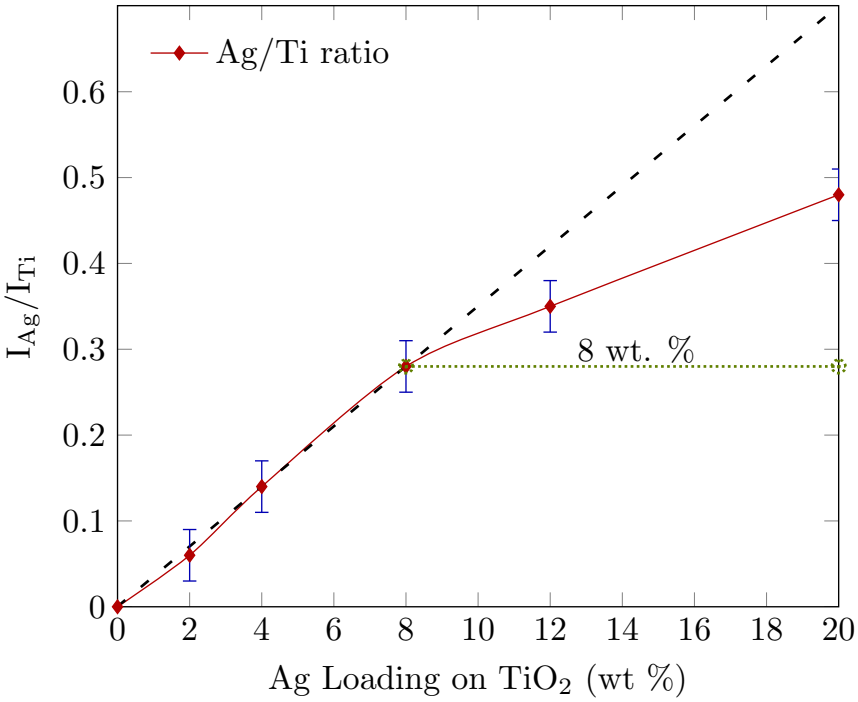

Figure 2.7: Ag/Ti ratio as a function of weight loading of Ag

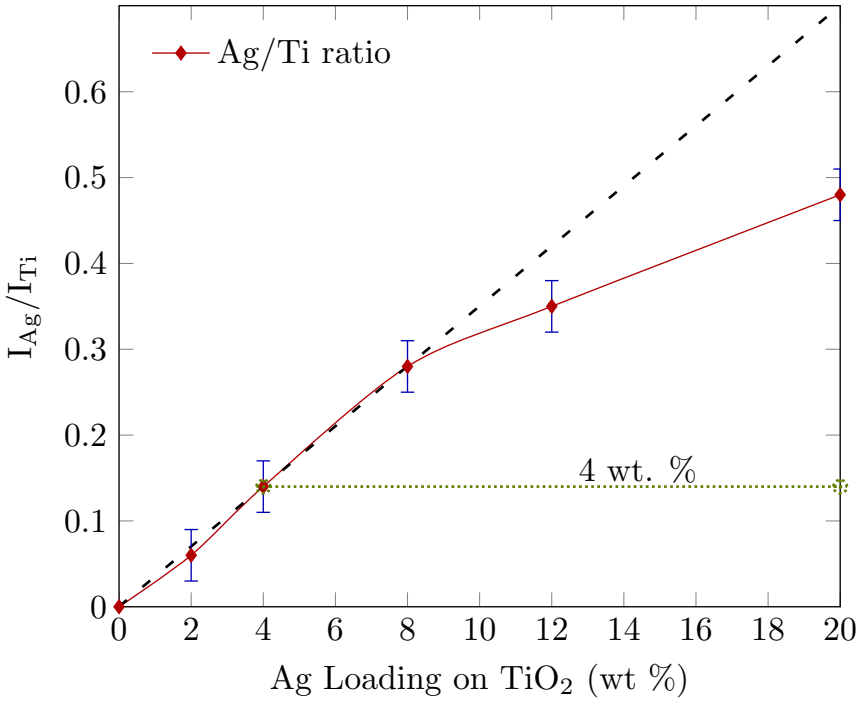

Figure 2.8: Ag/Ti ratio as a function of weight loading of Ag

Table 2.7: Particle Growth - after 8 wt% Loading

Ag	I_{Ag}/I_{TiO2}		Particle
Loading (wt%)	Experimental	Predicted	Size (nm)
8	0.28	—	0.35
12	0.35	0.39 ± 0.04	0.78
20	0.48	0.56 ± 0.07	1.03

Table 2.8: Particle Growth - after 4 wt% Loading

Ag	I_{Ag}/I_{TiO2}		Particle
Loading (wt%)	Experimental	Predicted	Size (nm)
4	0.14	—	0.35
8	0.28	0.24 ± 0.03	0.71
12	0.35	0.33 ± 0.04	0.84
20	0.48	0.46 ± 0.05	1.11

2.5 Conclusions of Previous Work

The ultimate goal of this project is to acquire a fundamental understanding of silver based desulfurization materials, in particular, Ag/TiO_2 adsorbents. A greater understanding of the surface properties responsible for the Ag/TiO_2 adsorbent's capacity to remove refractory sulfur compounds from high sulfur logistic fuels is necessary. This information is being sought to ultimately enhance performance capabilities and for the development of more efficient adsorbents. Previous studies have led to the conclusions stated below [5].

The following paragraphs in this section was taken from MSThesis.

The surface of the titania support from an XPS perspective is not appreciably shadowed by the Ag particles up to 20 wt% loading. The maximum area occupied by silver particle is less than approximately 6% of the total surface area of the titania assuming that the crystallites are evenly spaced of spherical, hemispherical or cubic geometries. Homogenous and mono dispersal of Ag on the support would result in coverage up to 0.81 ML at 20 wt%.

A functional relationship exists between the dispersed phase, the size of the silver particle and the observed XPS intensity. Ag/TiO_2 adsorbents display mono dispersion up to the 4 wt% loading. This corresponds to hypothesis that the silver atoms populate defects on the titanium support up to this specific weight loading. This 4 wt% loading is the critical loading baseline after which the atoms begin to grow into bigger crystallites. Refer to Figure 6.2 for illustration. The characteristic property of sulfur selectivity is a combination of the interaction of the silver oxide, the population of titania defects and the size of the silver crystallites. XPS result indicated the presence of Ag in its oxide form. The XPS oxygen peak due assigned to Ag^{1+} was the most dominant suggesting that Ag_2O was in the majority. XPS results also indicated that the activity of Ag/TiO_2 is most likely optimal not only for a specific size but also when the defects on the titania support are populated.

Oxygen chemisorption should not be used as the sole means of determining the particle size of Ag particles; the inherent assumptions may lead to inaccuracies in estimation. The combination of XPS and chemisorption measurements are a more accurate indication of the

actual crystallite size. Oxygen chemisorption over-estimated the particle size for Ag particles in the Ag/TiO_2 system studied. XPS provided a more accurate representation of particle size. The 20-100 nm particle size range estimated from XPS is supported by the fact that the Ag particle size could not be determined from XRD measurements, thus suggesting than the particle sizes are less than 5 nm.

Chapter 3

Experimental Methodology

3.1 Introduction

Surface characterization is of crucial importance to the advancement of adsorbent technology. Information received from the surface species can elucidate properties such as: composition, size, dispersion, reactivity, selectivity, active site, etc. The following sections briefly describe the theory involved in the application of the techniques utilized in this work.

3.2 X-ray Photoelectron Spectroscopy

X-ray photoelectron spectroscopy (XPS) is the most widely used surface sensitive characterization technique based on the photoelectric effect[44]. XPS give information about the chemical environment of a sample based on binding energy variation. When the surface of a sample is irradiated using an X-ray source, energy is transferred from the photons to the atoms on the surface of a sample. If the photon energy is enough to overcome the attractive forces binding the electron in its orbital, the electron will be emitted so that the atom can regain an energetically stable environment. The emitted electron, photoelectron, powered by the photon energy and kinetic energy are detected by an electron analyzer. Using the principle of conservation of energy,

$$h_\nu = E_k + E_b + \phi \tag{3.1}$$

where h_ν is the energy of the photon, E_k is the kinetic energy, E_b is the binding energy and ϕ is the work function.

The intensity of the photoelectronic peak for a sample as described by Penn [88] is

$$I = I_0 n \sigma \lambda(\epsilon) D(\epsilon) \tag{3.2}$$

where I_0 is the X-ray flux, n is the density of atoms, σ is the photoelectron cross-section, $\lambda(\epsilon)$ is the mean free path of energy (ϵ), $D(\epsilon)$ the fraction of electrons detected by the analyzer. More complicated forms of this equation exist as described by Briggs and Seah [89] which include more instrumental and morphological parameters; however, this form of the equation has a $\pm$ 10 % uncertainty which is deemed acceptable given the degree of difficulty in acquiring all the different parameters. This form of the equation is referred to as the 'first principle model' (FPM).

The experimental intensity, I,which corresponds to the area under the graph of the XPS peak, is used to determine the atomic concentration, C_x , of the element in the sample [90]:

$$A \propto C_x \sigma \lambda(\epsilon) D(\epsilon) \tag{3.3}$$

An empirical method using sensitivity factors can also be used to estimate C_x[79]:

$$C_x = \frac{\frac{I_x}{SF_x}}{\sum_i \frac{I_i}{SF_i}} \tag{3.4}$$

where SF_x is the atomic sensitivity factor for element x. The SF is directly proportional to the cross-section, the inelastic mean free path for the photoelectron core, level and several parameters that are dependent on the experimental conditions. Thus, all instrumental factors are grouped into the SF, which is given by Wagner et al. [78]:

$$SF = \sigma \phi y A T \lambda \tag{3.5}$$

where σ is the photoelectric cross-section for a particular transition cm^2, ϕ is the angular frequency factor, y is efficiency of production, A is the sample illuminated area, T is the detector efficiency, and λ is the mean free path of photoelectrons. A list of sensitivity factors are reported in the literature for a large number of elements using the F 1s line [78].

This method is however prone to lower accuracy than XPS measurement intensity derived from FPM [91]. Wertheim [90] states that there is no possibility of defining universally accepted applicable sensitivity factors. This is because the area of the main line that depends on the fraction of events accompanied by the multi-electron process varies among atoms and materials. Also, several issues arise for the transferability of SF between instruments. In this study, the FPM was applied to determine the atomic concentration.

3.2.1 Experimental

The XPS system consists of a non-monochromatic Leybold-Heraeus LHS-10 spectrometer with a dual anode Al/Mg X-ray source and hemispherical electron energy analyzer (HSA). XPS measurements were taken with an X-ray source typically requiring between 100 W and 350 W of power. The system typically yielded a 1.2 eV FWHM for the Au($4f_{7/2}$) photoelectron peak of a gold foil using a Mg Kα anode at a workable spectrometer pass energy and count rate. The measurement uncertainty was recorded as $\pm$ 0.2 eV. The samples were mounted on carbon, high-vacuum compatible, double-sided adhesive tape. Sorbent samples were introduced into the load lock and degassed to pressures of ca. 1 $\times 10^{-6}$ Torr. Subsequently, the samples were inserted into the main chamber where measurements were taken at a residual pressure of ca. 1 $\times 10^{-7}$ Torr. Al Kα (hν =1486.6 eV) or Mg Kα (hν =1253.6 eV) x-ray source was used at spectrometer operating conditions of 10 mA and 50 eV. XPS data were fitted using the XPSPEAK41 program. Sample charging was compensated for by adjusting XPS settings to the C 1s peak at 284.6 eV. The samples were assessed to ensure that the shoulder was not the result of artifacts due to system contamination. Atomic ratios

were derived using the analysis of the elemental peak areas following well established methods for XPS data analysis [48, 52, 78, 88–90, 92]. Peak deconvolution was performed using a nonlinear Shirley baseline and a combination of Gaussian and Lorentzian type curves.

3.3 Oxygen Chemisorption

Chemisorption is an analytical adsorption technique (widely used in heterogenous catalysis) that is based on chemical interactions occurring between the the adsorbate gas and the exposed surface of a catalytic material. Chemisorption is used to reveal information about a variety of surface properties. These include but are not limited to: the active metal surface area, dispersion of the active metal, surface energy, reducibility and oxidizability of the catalytic material, and crystallite size. In this work, information from selective oxygen chemisorption was used specifically to determine the silver crystallite size of the Ag/TiO_2 adsorbent. Oxygen gas was used in preference to other gases such as CO and H_2 as it most readily adsorbed to form a well-defined monolayer coverage (with the least challenges) [38, 93–95].

Selective oxygen chemisorption was used to obtain the active metal surface area at conditions which supported the formation of a monolayer on the surface of the exposed metal atoms. The number of surface metal atoms is obtained from measuring the amount of chemisorbed gas. The amount of oxygen chemisorbed based on the formation of a monolayer was used with the known adsorption stoichiometry between the adsorbate gas and the metal [38, 40, 41, 96, 97]. The metal surface area is given by:

$$ASA = \frac{N_m \cdot S \cdot A_m}{166} \tag{3.6}$$

where ASA is the active surface area of the metal atoms (m^2/g), N_m is the oxygen monolayer uptake (moles/g), S is the adsorption stoichiometry, and A_m is the cross-sectional area of the active metal surface atom, which is 8.696 ($Å^2$/ Ag atom).

Metal crystallite size was determined by estimating the volume from the mass and the density of the supported metal, using the ASA, and by assuming a geometry of the crystallite. The geometries assumed were (i) spherical, (ii) hemispherical, and (iii) cubic. The average crystallite size is given by:

$$d = \frac{L \cdot f}{ASA \cdot \rho_m} \tag{3.7}$$

where d is the particle diameter, L is the percent metal loading, ρ_m is the density of the supported metal, and f is the particle shape correction factor ($f = 6$ for spherical and hemispherical particles and $f = 5$ for cubic particles).

The metal dispersion D, which is the ratio of exposed active metal to the total number of metal atoms in the sample material is given by:

$$D = \frac{N_A \cdot N_m \cdot m_s \cdot S \cdot MW}{L \cdot m_s \cdot N_A} \tag{3.8}$$

where MW is molecular weight of the metal and m_s mass of sample. The equation is reduced to:

$$D = \frac{N_m \cdot S \cdot MW}{L} \tag{3.9}$$

3.3.1 Experimental

The Quantachrome Autosorb-1 was used to perform oxygen chemisorption using that static chemisorption technique [95]. Three pretreatment steps were carried out for oxygen chemisorption: firstly, $\sim$ 5 mg of the adsorbent pellets were heated to 150°C followed by an evacuation at 2.99 $\times$ 10^{-9} Torr for 30 minutes to remove the moisture and contaminants from the surface. Secondly, hydrogen reduction at 300°C and 760 Torr for 60 minutes to provide reducible oxygen uptake. Thirdly, evacuation at 300°C and 2.99 $\times$ 10^{-9} Torr for 60 minutes for the removal of physisorbed hydrogen. Oxygen uptake was recorded at 170°C after saturation of the surface was reached. The Brunaur-Emmett-Teller (BET) surface areas

were measured from nitrogen gas adsorption-desorption at 77 K. The average sizes of the dispersed crystallites were derived from the active surface area.

3.4 Electron Paramagnetic Resonance

Electron Paramagnetic Resonance (EPR) is a spectroscopic technique that is used to detect chemical species that have unpaired electrons. It is the measurement and interpretation of the energy differences between the atomic or molecular states and is used to increase knowledge about the structure of molecules and probe the adsorbate-surface interactions by analyzing a molecular absorption spectra which arise when the frequency and the amount of the electromagnetic radiation is changed as it passes through a sample.

EPR is based on the interaction of electromagnetic radiation with magnetic moments arising from electrons. In EPR the intensity, the number of absorption lines and the line position is used to identify different nuclei. Intensity is purely a property of the electron,but can be correlated to a metal when the metal content is known.

Line positions in EPR are stated in g values which is a function of the ratio of the frequency to the resonant field. The relationship describing the absorption of microwave energy between two spin states is

$$\Delta E = h\nu = gbB$$

where:

ΔE is the energy difference between the two spin states

h is Planck's constant

ν is the microwave frequency

g is the Zeeman splitting factor

b is the Bohr magneton

B is the applied magnetic field.

EPR can identify an absorption site via superhyperfine structure (observable only when nonzero nuclear spins are present) or **g** tensor. EPR is used as a complementary technique to characterize the adsorbate surface system, information can only be obtained if the system is paramagnetic. Thus, in the $AgTiO_2$ system we can only gain direct information on the Ag^{2+} paramagnetic species and the Ti^{+1} signals.

3.4.1 Experimental

The EPR system consists of a Bruker EMX-6/1 X-band EPR spectrometer composed of: an EMX 1/3 console, an ER 041 X61 bridge microwave bridge with built-in microwave frequency counter, an ER070 magnet, and an ER-410410st standard universal rectangular angular cavity. Data acquisition was performed with the software supplied by Bruker (WINEPR acquisition program), data manipulation (determination of g-values, subtraction, base lining, integration and conversion to ASCII files for use with Origin or Microsoft Excel) was done with the WINEPR program version 2.11.

Ag/TiO_2 samples were prepared by the method described previously in Section 2.1.1. Prepared samples were cooled with liquid nitrogen to 77 K in a finger Dewar. Spectra of the as-prepared sorbent were recorded with a field modulation frequency of 100 kHz, a modulation amplitude of 10 mT, a frequency of 9.37 GHz, and a power supply of 2 mW.

3.5 Inductively Coupled Plasma Atomic Emission Spectroscopy

Inductively Coupled Plasma Atomic Emission Spectroscopy (ICP-AES) is a high specificity, multi-element analytical technique used for elemental composition. Inductively coupled plasma is used to excited electrons to higher energy levels and upon returning to the ground states, these electrons emit energy at a given wavelength. By comparing the emission wavelength and intensity the element and the concentration of can be determined relative to a reference standards. The quality of the chemical composition of the Ag/TiO_2 adsorbents was confirmed using inductively coupled plasma atomic emission spectroscopy. The silver

concentration was quantified against certified standards using spectral line 328.068 nm. A minimum of three measurements were taken for each sample.

3.5.1 Experimental

Samples were ground with a mortar and pestle, weighed to 0.1 g and digested using EPA Method 3051A, which is a microwave digestion procedure to extract total elements. Microwave digestion was performed on a Mars Xpress system (CEM Corporation, NC) with 10 mL of concentrated nitric acid. Digested samples were filtered and the volume made up to 100 mL with deionized water. Samples were analyzed using ICP-OES (Spectro Ciros ICP, SPECTRO Analytical Instruments, Kleve, Germany).

Chapter 4

Adsorption Studies

The following studies were performed to contribute to a complete understanding of Ag/TiO_2 adsorbents.

4.1 Chemisorptive Properties of Ag/TiO_2 Adsorbents

There are inconsistencies in the particles sizes resulting from determination using XRD, XPS, and oxygen chemisorption. Particle size could not be evaluated using XRD for weight loading ranging from 0–20 wt% Ag/TiO_2. Silver was detected at the 20 wt% loading but could not be quantified due to its small concentration. Particle sizes determined using XPS and oxygen chemisorption are listed in Table 4.1

Table 4.1: Comparison of Oxygen Chemisorption, XPS, and XRD Particle Size

Ag	Particle Size (nm)		
wt% Loading	O. C.	XPS	XRD
4	3.4	0.35 ± 0.03	ND
8	4.1	0.71 ± 0.03	ND
12	5.3	0.84 ± 0.03	ND
20	6.9	1.11 ± 0.03	*D

ND - not detectable,

*D - detectable but not quantifiable

The particle sizes calculated from XPS were considerably smaller than those derived using oxygen chemisorption. XRD did not provide conclusive measurements when applied

in the crystallite size determination of Ag/TiO_2 adsorbents. The lack of signal suggested that the crystallite was below the detection limit of the XRD $\lessapprox$ 5 nm [30–32]. This supports the validity of the XPS particle size determination.

Suppression of oxygen results in an overestimation of particle size. There are several factors that could have resulted in the particle size exaggeration using oxygen chemisorption. These factors are built into the assumptions and biases of the techniques and were discussed in Chapter 2. In an effort to resolve the inconsistencies in calculated silver particle size by oxygen chemisorption, the following experiments were performed:

Part 1 - Evaluation of TiO_2 native oxygen uptake

The oxygen uptake on native or nitrated TiO_2 surface was determined for previously reported particle sizes determined by oxygen chemisorption [22]. The particle sizes were re-evaluated and corrected for the native uptake on the adsorbent in the absence of silver particles. Repeated measurements were performed to eliminate random error. The native O_2 uptake was found to be 8.38 $\pm$0.15 μmol/g. There was negligible difference in uptake between native TiO_2, nitrated TiO_2 and the particular nitrate loading of TiO_2. Supporting data can be seen in Table 4.2. The average particle sizes increased by 0.2 nm when re-evaluated for the native oxygen uptake see Table 4.3. However, consideration of the native uptake of TiO_2 cannot account for the exaggerated particle size, on the contrary, particle size is increased.

Table 4.2: Evaluation of Blank TiO_2 Oxygen Monolayer Uptake

	Monolayer Uptake (Nm) (μmol/g)			
Sample	Run 1	Run 2	Run 3	Average
0wt-NO_3−TiO_2	9.736	9.085	6.907	8.576
4wt-NO_3−TiO_2	7.777	8.646	8.425	8.283
7.2wt-NO_3−TiO_2	8.271	7.947	8.674	8.297

Table 4.3: Comparison of Particle Size Uncorrected and Corrected for Native TiO_2 Uptake

Average	Ag wt% Loading				
Particle Size (nm)	0	4	8	12	20
Uncorrected Blank	0	3.4	4.1	5.3	6.9
Corrected Blank	0	3.6	4.3	5.5	7.1

Accounting for the native TiO_2 uptake for Ag loadings less than 4 wt% results in a more significant increase in particle size. Provided that all the assumptions are consistent for the various weight loadings, at the lower loadings monolayer uptake is lower, thus the constant value which the native uptake is, would have a greater impact in the determination of particle size. Examining the chemisorption particle size determination equation, eqn 4.1, particle diameter is inversely proportional to the monolayer uptake. Thus, when monolayer uptake decreases particle size increases. Also, consider the fact that a smaller number in the denominator of a fraction gives a greater result.

$$d = \frac{100 \cdot L \cdot f \cdot 166}{N_m \cdot S \cdot A_m \cdot \rho_m} \tag{4.1}$$

In the chemisorption particle size determination equation, Equation 4.1, d is the particle diameter, L is the percent metal loading, ρ_m is the density of the supported metal, f is the particle shape correction factor, N_m is the oxygen monolayer uptake (moles/g), S is the adsorption stoichiometry, and A_m is the cross-sectional area of the active metal surface atom (Å/ Ag atom).

In Table 4.4, 1–2 wt% Ag/TiO_2 was reproduced and the monolayer uptake was determined. This table shows the significant impact that the native uptake has on lower weight loadings. The evaluation of 1–2 wt% Ag/TiO_2 resulted in the hypothesis that oxygen is being suppressed during chemisorption. The following experiments will seek to determine the cause of this suppression.

Table 4.4: Effect of Native TiO_2 Oxygen Uptake at Ag loading Less than 4 wt%

	Ag wt% Loading			
	1	1	2	2
Monolayer Uptake (Nm) [μmol/g]	28.72	24.67	44.70	46.71
Average Crystallite Size [nm]	3.80	4.42	4.88	4.67
Corrected for Native TiO_2 uptake				
Monolayer Uptake (Nm) [μmol/g]	20.43	16.38	36.41	38.42
Average Crystallite Size [nm]	5.34	6.66	5.99	5.68

Part 2 - Investigation into the Suppression of Chemisorbed Oxygen of Ag crystallites on TiO_2 support

In chemisorption, monolayer capacity is defined as the amount of adsorbate which is needed to occupy all adsorption sites as determined by the structure of the adsorbent and by the chemical nature of the adsorptive gas. Several factors are known to affect monolayer uptake, namely, reduction temperature, SMSI interactions and strongly bonded subsurface oxygen. Additionally, suppressed oxygen uptake for very small particles have been noted for metals such as, platinum, rhodium, and iridium. Perhaps there is a similar occurrence in silver, where it is believed that the enhanced affinity of the small particles is dominant relative to the electron transfer need to the adsorbed oxygen [36].

Note: Weak chemisorption was not performed because there is no difference between weak and strong chemisorption suggesting that the negligible influence from weak chemisorption.

(i) The Effect of Reduction Temperature

Ag/TiO_2 particles sizes stated in previously in Nair et al [22], were evaluated when hydrogen reduction was performed at 300 °C. This, in direct contrast to thermo-reduction profiles of Ag/TiO_2 adsorbents with various loadings of silver, which reported reduction temperatures at temperatures as high as 340 °C as seen in Table 4.5 and Figure 4.5. Likewise, Schön et al [76], and Hammond et al [77], showed that silver oxides were reduced after 300 °C ; reduction of the Ag_2O was shown at 320 °C and 380 °C respectively.

This study seeks to confirm the hypothesis that oxygen chemisorption is inhibited at 300 °C. Performing reduction at 400 °C would be more appropriate for oxygen chemisorption to ensure greater reduction of the silver oxides. It has been shown that low temperature reduction of TiO_2 supported metal has led to suppression when reduction occurred at 500 °C as opposed to 200 °C [99]. The adsorption of oxygen will be monitored as a function of hydrogen reduction temperature.

Table 4.5: Ag/TiO_2 hydrogen reduction temperature using TPR technique

Ag Loading	Hydrogen Reduction Temperature		
(wt%)	$T_{1\,max}$(°C)	$T_{2\,max}$(°C)	$T_{3\,max}$(°C)
1	102	146	292
2	103	140*	341
3	102	146	292
4	114	140*	339
5	129*	153	328
6	108	140*	313
10	106	171	322

(ii) Strong Metal Support Interactions (SMSI) metals are polarized by the highly charged cations of surface oxides. Strong metal-support interaction is a term used to describe

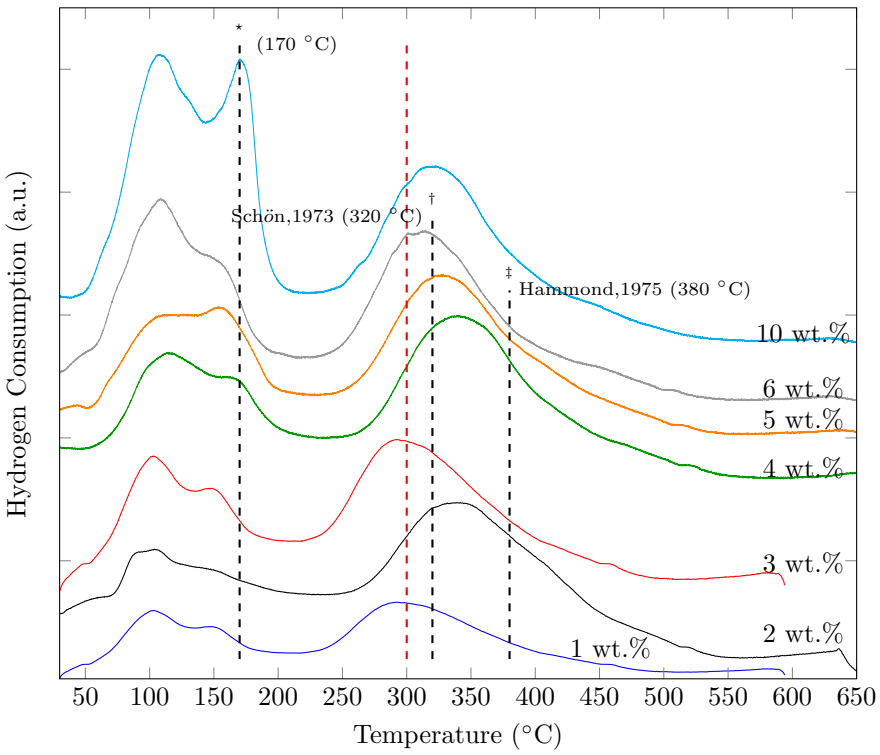

Figure 4.1: Temperature Programmed Reduction profiles of various loadings Ag/TiO_2 samples.

the drastic changes that occur in the chemisorption properties of group VIII (8-10) metals when they are dispersed on the surfaces of transition metal oxides [100]. The ability to chemisorb probe molecules is either suppressed or absent.

Classical SMSI effect as noted by Tauster et al [101], was discovered on group VII metals supported on TiO_2. Thus, it is likely that Ag/TiO_2 adsorbents have strong metal-support interactions due to the fact that they display atypical chemisorption properties and have superior activity and selectivity. Traditionally, Ag encapsulation by TiO_2 and electron transfer would be indicative of SMSI from Ag to TiO_2. In the process of encapsulation or decoration, the lower oxides of titanium would migrate unto the silver particles, thereby blocking the active sites of the metal particles inhibiting chemisorption. SMSI due to charge transfer would be as a result of a change in the silver charge due to the interaction with the titanium metal ions. However, in a series

experiments where silver/titania was reduced at 550°C silver did not exhibit characteristics that were usually attributable to SMSI [102]. These experiment may not be related because the size of the silver particle are larger than particles present in our current Ag/TiO_2 system. Real time XPS studies mimicking chemisorption conditions could show these electron charge interactions.

4.2 Investigation of the Chemisorption Stoichiometric Ratio between Silver and Oxygen

The accuracy of the chemisorption technique relies on a variety of background information. These include the correct stoichiometric ratio, the ability of an absorbate gas to selectively chemisorb on the active metal, and constant gas uptake on the support when the metal is present or absent. For the Ag/TiO_2 adsorbent, there may be problems due to the variation in the stoichiometry ratio of Ag : O (the number of sites per chemisorbed oxygen atom) at the adsorption surface [37]. Although $Ag_{(S)} : O \simeq 1$ appears to be the best value, as reported in the literature [38–40], other stoichiometries possibilities have been reported [38, 40, 41, 96, 97]. Table 4.6 lists some of the Ag/O stoichiometric ratios reported for oxygen chemisorption in the literature. Differences in stoichiometries may be due to the hypothesis that the gas molecule to metal stoichiometry is dependent on metal particle size. Other discrepancies may result from either the complex oxygen adlayer [41, 42] or carbonaceous contaminants, which have an effect on the sorption behavior of oxygen due to possibility of subsurface oxidation of silver [38].

In chemisorption, there is size variation depending on the crystallite geometry assumed. For example, spherical and cubic geometries will produce slightly different average dimensions. Other problems, that may arise, include multiple adsorption of oxygen molecule on metal surface atoms, internal absorption, incomplete adsorption of the oxygen molecules by the metal particles, and non-metallic silver particles. Of these problems, explanations for exaggerated crystallite size would be adsorption by titania support – subsurface adsorption and multiple adsorption of gas molecule on metal surface atoms – under estimation of the stoichiometric ratio [43]. Lower crystallite size would result from over estimation of the stoichiometric ratio and inability of absorbate gas to selectively chemisorb a monolayer.

In this investigation the stoichiometric ratio was varied to explore which which ratio more accurately describes the system and conforms to the chemistry and findings of supporting characterization techniques.

Table 4.6: Ag/O stoichiometric ratio reported for chemisorption

Compound	Ag/O ratio	Size	Adsorption Temperature °C	Technique	Reference	Year	Notes
Ag/corundrum, Ag/porcelain	<1, 1		200	O.C.	Kholyavenko et al [40]	1954	
Ag catalysts	1		180–300	O.C.	Smeltzer et al. [96]	1956	
Ag powder	1		-77 to 350	O.C.	Czanderna [41]	1964	
Ag/γ, α-Al_2O_3	1	> 50 Å	50, 100, 150, 170, 200	O.C.	Scholten et al [39]	1973	
Ag/α-Al_2O_3	1		200	O.C.	Verykios et al [97]	1980	
Ag powder	0.9–1.1		180	O.C.	Kagawa et al [103]	1982	
Ag/α-Al_2O_3	1		170	O.C.	Strohmayer et al [38]	1983	
Ag powder, Ag/SiO_2, Ag/TiO_2	1		170	O.C.	Seyedmonir et al [37]	1984	
Ag/γ-Al_2O_3	2		170	O.C.	Hoost et al [104]	1997	
Ag/Al_2O_3	1		170	O.C.	Yeung et al [105]	1998	
Ag/Al_2O_3	2		170	O.C.	Arve et al [106]	2006	
Ag powder, Ag/α-Al_2O_3							

O.C.– Oxygen Chemisorption

The trend in oxygen uptake for various loadings Ag/TiO_2 samples is shown in Figure 4.2. On observing the variation in trend in Figure 4.2 quality of the silver weight loading was checked with ICP and the corresponding weight loadings were adjusted to chemical composition reported by ICP. The value initially reported as 1 wt% loading was found to more closely represent 2 wt% and 12 wt loading was discard as it failed the 95 % confidence interval. Increased oxygen absorption maybe to an extra carbonaceous content. This curve is remarkably similar in shape to Figure 2.8 which displays Ag/Ti ratio as a function of weight loading. Thus, fundamental the raw data, the monolayer up and the Ag/Ti ratio offers the same trend and the analysis breaks with chemisorption when the assumptions are applied, such as stoichiometric ratio.

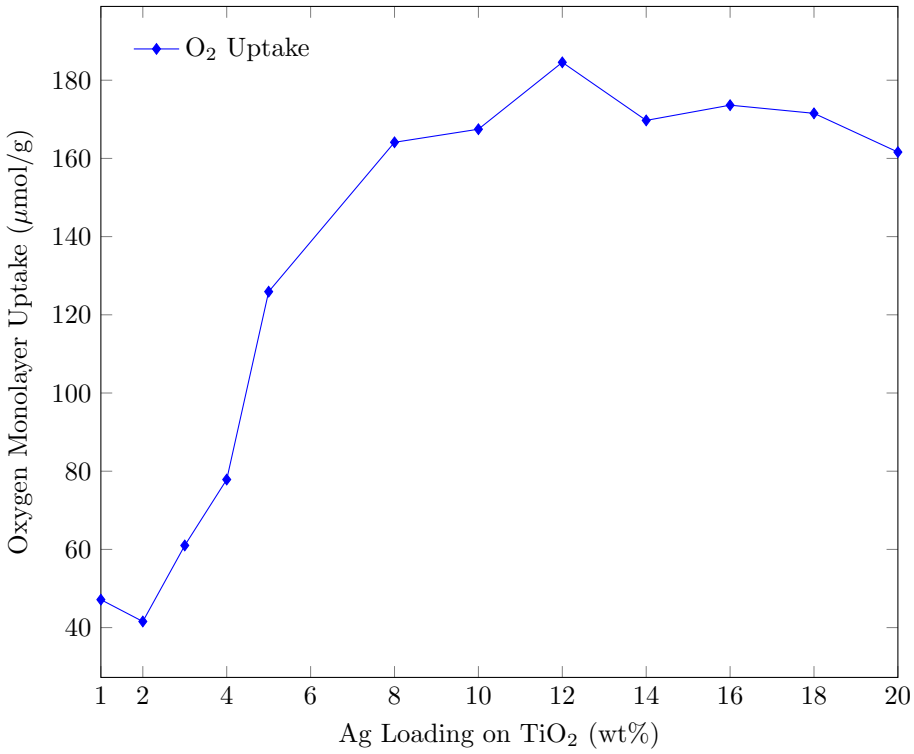

Figure 4.2: Trend in Oxygen Uptake for Various Loadings Ag/TiO_2 Samples.

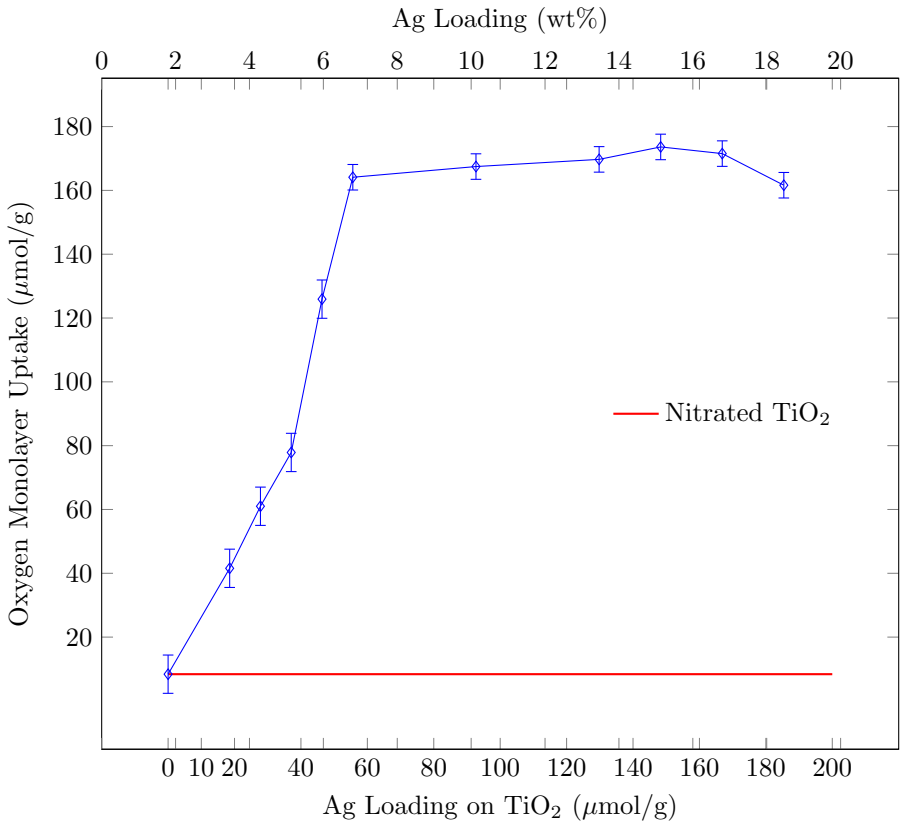

Figure 4.3: Trend in Oxygen Uptake for Various Loadings Ag/TiO_2 Samples.

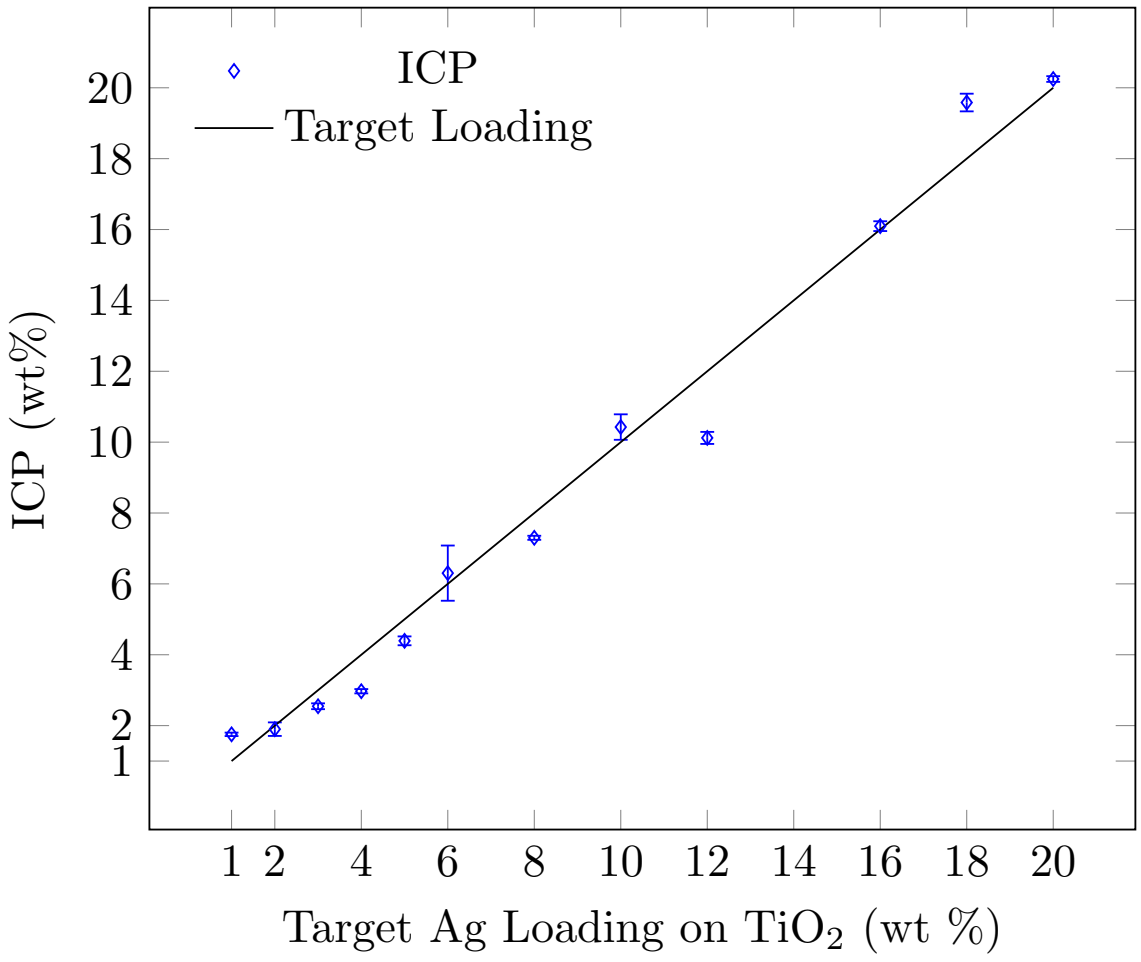

Figure 4.4: ICP Ag composition as a function of target preparation for Ag on TiO_2

Table 4.7: Oxygen Chemisorption Results with an Ag/O Ratio of 1 for x %wt Ag/TiO_2 Adsorbent

Ag Loading (wt%)	Monolayer Uptake (mol/g)	Active Metal Surface Area (m^2/g)	Percent Metal Dispersion (%)	Average Crystallite Size (nm)
2	47.15	2.47	23	5.11
2	41.56	2.18	22	5.25
3	61.01	3.20	22	5.36
4	77.87	4.08	21	5.60
5	125.92	6.60	27	4.33
8	164.12	8.60	22	5.32
10	167.47	8.77	18	6.51
14	169.72	8.89	13	9.00
16	173.62	9.10	12	10.1
18	171.53	8.99	10	11.4
20	161.62	8.47	9	13.5

Table 4.8: Oxygen Chemisorption Results with an Ag/O Ratio of 2 for x %wt Ag/TiO_2 Adsorbent

Ag Loading (wt%)	Monolayer Uptake (mol/g)	Active Metal Surface Area (m^2/g)	Percent Metal Dispersion (%)	Average Crystallite Size (nm)
2	47.15	4.94	46	2.55
2	41.56	4.35	45	2.62
3	61.01	6.39	44	2.68
4	77.87	8.16	42	2.80
5	125.92	13.19	54	2.17
8	164.12	17.20	44	2.66
10	167.47	17.55	36	3.23
14	169.72	17.78	26	4.50
16	173.62	18.19	23	5.03
18	171.53	17.97	21	5.72
20	161.62	16.93	17	6.75

Table 4.9: Oxygen Chemisorption Results with an Ag/O Ratio of 0.5 for x %wt Ag/TiO_2 Adsorbent

Ag Loading (wt%)	Monolayer Uptake (mol/g)	Active Metal Surface Area (m^2/g)	Percent Metal Dispersion (%)	Average Crystallite Size (nm)
2	47.15	1.23	12	9.25
2	41.56	1.09	11	10.50
3	61.01	1.60	11	10.72
4	77.87	2.04	10	11.21
5	125.92	3.30	14	8.66
8	164.12	4.30	11	10.63
10	167.47	4.39	9	13.03
14	169.72	4.44	7	18.00
16	173.62	4.55	6	20.10
18	171.53	4.50	5	22.89
20	161.62	4.23	4	26.99

The Ag/O stoichiometric ratios, 1, 2 and 0.5 were applied to the oxygen chemisorption analysis. Stoichiometric ratios 1 and 2, because they are the most frequently reported in literature and 0.5 to explore the possibility. Tables 4.7, 4.8 and, 4.9 list the values obtained for active metal surface area, metal dispersion and the average crystallite size derived from the oxygen uptake. The average crystallite sizes and the metal dispersion are plotted in Figures 4.5. As expected these values exhibit a strong dependence on the stoichiometric ratios. Average crystallite size increases with increasing Ag/O ratio while metal dispersion decreases with Ag/O ratio.

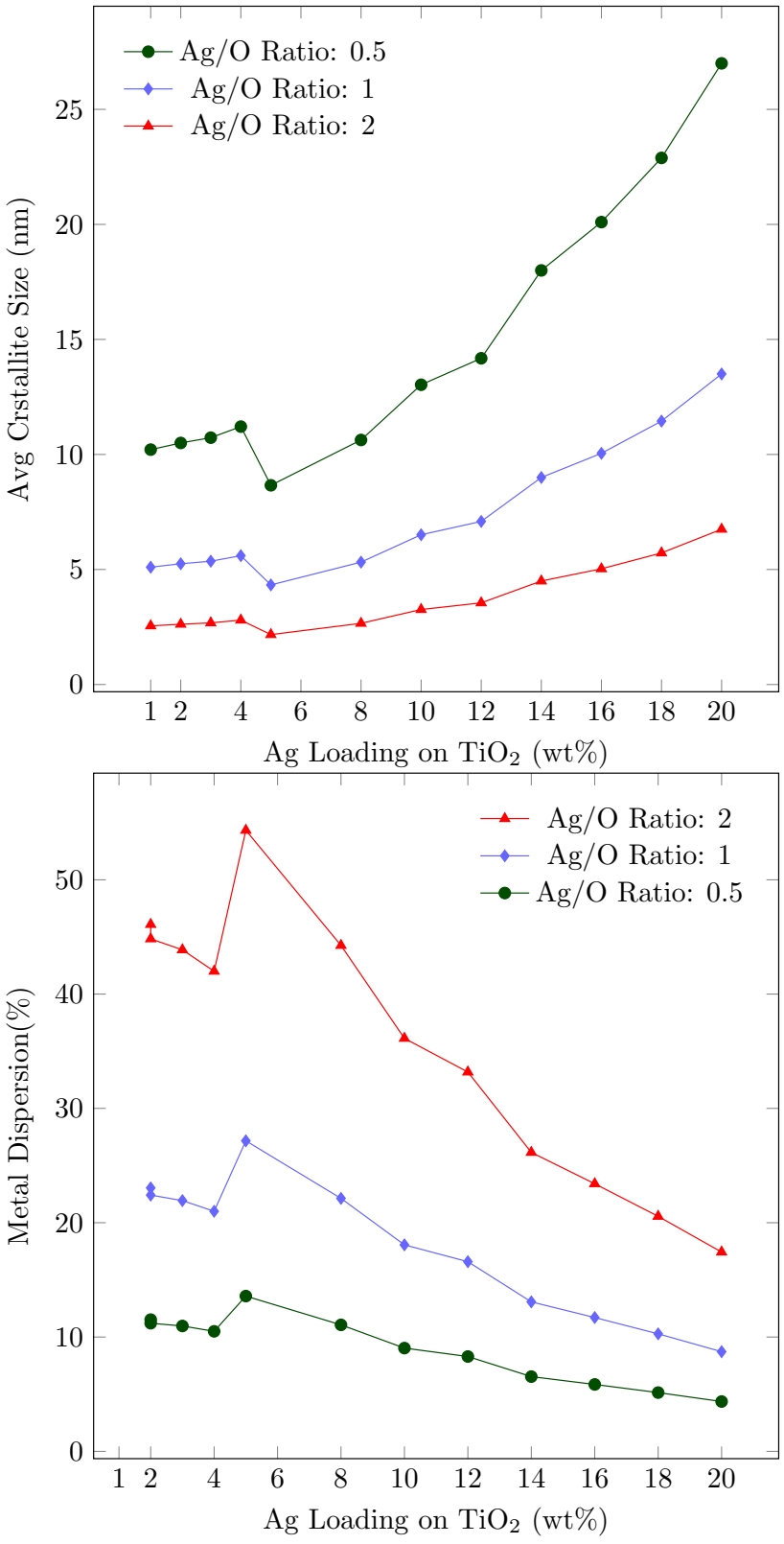

Figure 4.5: Average Crystallite Size and Dispersion Dependency on Ag/O Stoichiometric Ratio

Chapter 5

TPR

5.1 Temperature Programmed Reduction (TPR)

Temperature Programmed Reduction (TPR) is a sensitive technique which depends on the property of reducibility of the system under study. At a specific temperature, a peak is generated corresponding to the reduction of an oxide. The reduction temperature of an active site may vary depending on the oxidation state of a metal. During reduction, oxygen ions at the reaction interface are removed by the inward diffusion of hydrogen and the outward diffusion of oxygen. Eventually, the metal nuclei will grow until there is complete removal of the oxide. In this study, TPR was performed using a 5% H_2 95% He gas stream (15 ml/min) in a flowing reaction system in a tube furnace. 0.100 g of Ag/TiO_2 was linearly heated from 30 °C to 650 °C at a rate of 10°C/min. A thermal conductivity detector (TCD) was used to measure the differences in thermal conductivities of the gas stream. The TCD signal was calibrated and CuO was used to calibrate the number of moles of H_2 consumed. The area under the peak of a concentration versus time or temperature graph was integrated to give the total H_2 consumed from reduction. A more detailed experimental procedure is presented in the Experimental Section. Precise control over experimental variables is necessary for accurate data comparison. TPR is affected by particle size of the sample, heating rate, concentration of gas stream and, the gas flow rate. The reaction between the silver titania system and hydrogen is represented by the equation

$$AgO(s) + H_2(g) \longrightarrow Ag(s) + H_2O(g)$$

$$Ag_2O(s) + H_2(g) \longrightarrow 2\,Ag(s) + H_2O(g)$$

The Gibbs free energy is negative for Ag_2O which indicates thermodynamic feasibility.

The objective of the study is to examine the redox behavior of Ag/TiO_2 using hydrogen as a reducing agent in order to evaluate the assumptions made using oxygen chemisorption. This is a part of a larger investigation to correlate XPS findings with the results from oxygen chemisorption.

Experimental

TPR experiments were performed in a quartz fixed bed flow reactor (4 mm i.d.) connected to a SRI 310C gas chromatograph. A sample size of approximately 100 mg held between two layers of quartz wool was loaded into a the reactor. The temperature controller was connected to a thermocouple in contact with the quartz reactor directly outside the location of the sample. The sample was pretreated in air for 30 mins at 115 minutes to remove water vapor, then cooled to room temperature in Ar. Argon was allowed to flow at 15 ml/min for 30 mins. Reduction was performed using a 5% H_2 95% He gas stream flowing at (15 ml/min) and through a temperature range of 30 °C to 650 °C at a rate of 10°C/min. The H_2 consumption was monitored using a TCD detector and CuO was used as reference compound. A schematic of the system used for TPR is shown in Figure 5.1.

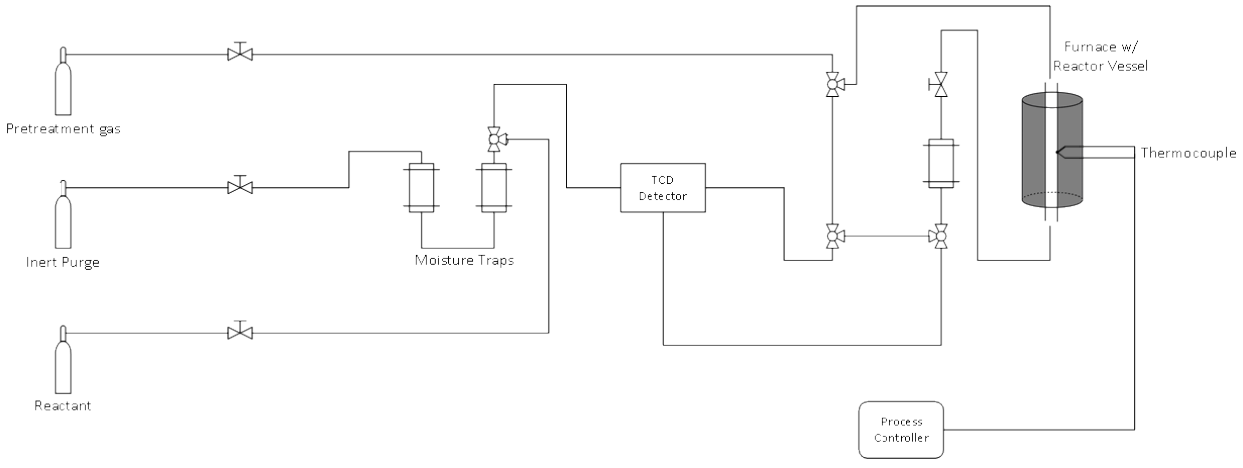

Figure 5.1: Schematic of Temperature Programming Reduction Setup

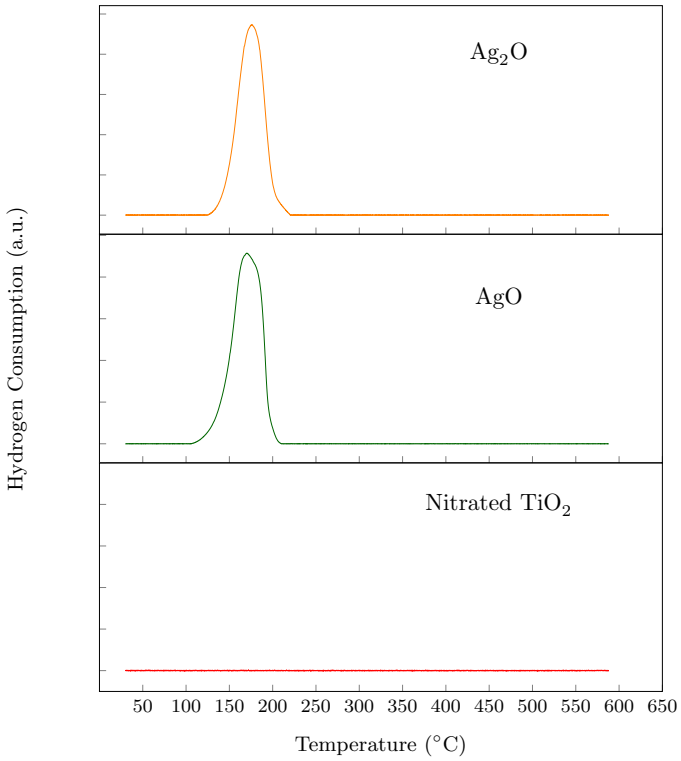

Figure 5.2: Temperature reduction profile (10 °C/min) for reference compounds Ag_2O, AgO, and nitrated TiO_2

Table 5.1: Temperature reduction analysis of reference compounds

Sample	T_{max} (°C)	H_2 Consumption (μmoles/g)
AgO	170	665.3
Ag_2O	176	308.8

Results and Discussion

The study describes the reducibility of Ag/TiO_2 using TPR as a function of Ag content. Figure 5.2 shows the TPR patterns of crystalline reference compounds used in an attempt to locate and isolate characteristic signals. 10.0 mg of AgO and Ag_2O, and 100 mg of Nitrated TiO_2 was used for sample reference analysis. The ratio of hydrogen consumption for AgO and Ag_2O was confirmed to be 2. The TPR-H_2 pattern of nitrated TiO_2 exhibited no defined peaks that could be attributed to the reduction of the TiO_2 support. This indicated that Ag_xO (Alfa Aesar, 98% metal basis) in Ag/TiO_2 could be fully reduced by H_2. AgO (Alfa Aesar, 99+% metal basis) showed a maximum reduction peak temperature (T_{max}) at 170 °C, while Ag_2O had a (T_{max}) at 176 °C.

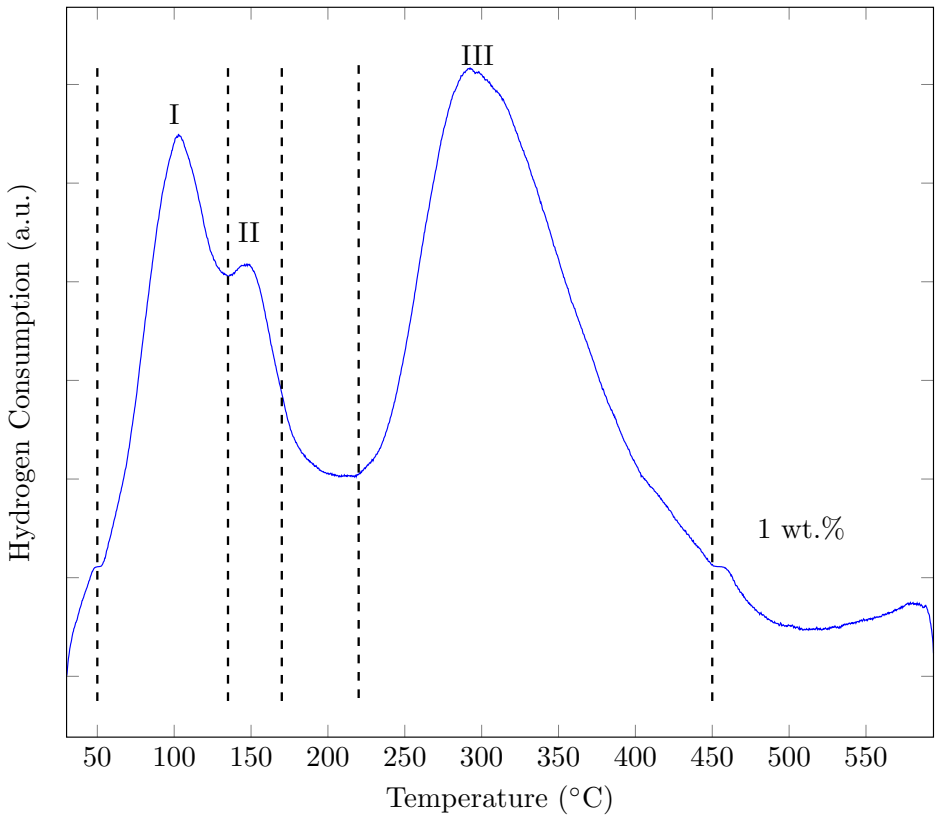

Figure 5.3: Temperature reduction profile for 1 wt%Ag/TiO_2 showing the phase of reduction

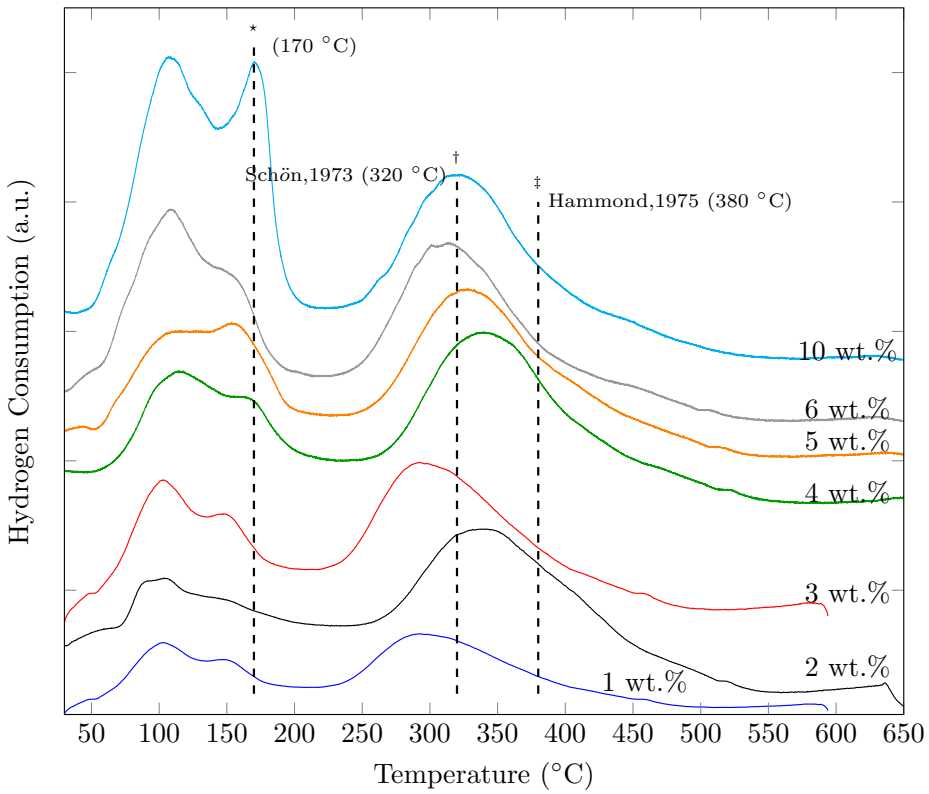

Figure 5.4: Temperature reduction profile for various loadings of Ag/TiO_2

The reduction profile in Figure 5.3 shows the three phases into which a typical loading is divided into for discussion (1wt% loading was used for illustration):

- Phase I (100–110°C): peak attributable to Ag_xO reduction
- Phase II (140–170°C): peak attributable to Ag_xO reduction
- Phase III (290–340°C): peak attributable to Ag_xO reduction

The first two peaks (phase I & phase II) are clearly present in the temperature range of 100–180 °C, known range for hydrogen consumption by AgO and Ag_2O. The H_2 consumption increases with increased Ag loading. All three peaks characteristic to hydrogen reduction of Ag/TiO_2, thus can be ascribed to the reduction of the Ag species. Increasing the Ag loadings increased each of the three phases, see in Figure 5.4. The three characteristic features was independently confirmed by Quantachrome Laboratory see Figure 5.5. There is a definite shift in the ratio of the particular species of Ag as demonstrated by the values for the ratio

of Phase 1: Phase 2 in Table 5.2. Phase II is hypothesized to be linked to the metallic character of silver. It grows significantly at higher weight loadings.

The negative peak seen in the hydrogen TPR analyses is indicative of hydrogen desorbing off of the sample at higher temperatures. A mass spectrometer attached to the instrument is needed to precisely determine elution at each peak. Figure 5.6 displays the moles of Ag reduced assuming Ag^{+2} and Ag^{+1} to Ag^{0}. The diagonal line indicates the number of moles theoretically available for reduction assuming all Ag species are reducible. Since it is theoretically impossible for Ag^{+1} to be above the diagonal line, the results suggest that the Ag^{+1} may not be the dominant in Ag/TiO_2 system. However, this is in contrast to previous XPS and EPR investigations [28]. There are several ways to explain the over estimation of the number of moles of Ag^{+1}:

- Different Ag^{x} species exist on Ag/TiO_2 in different ratios and different weight loadings
- Species are consuming more H_2 than expected

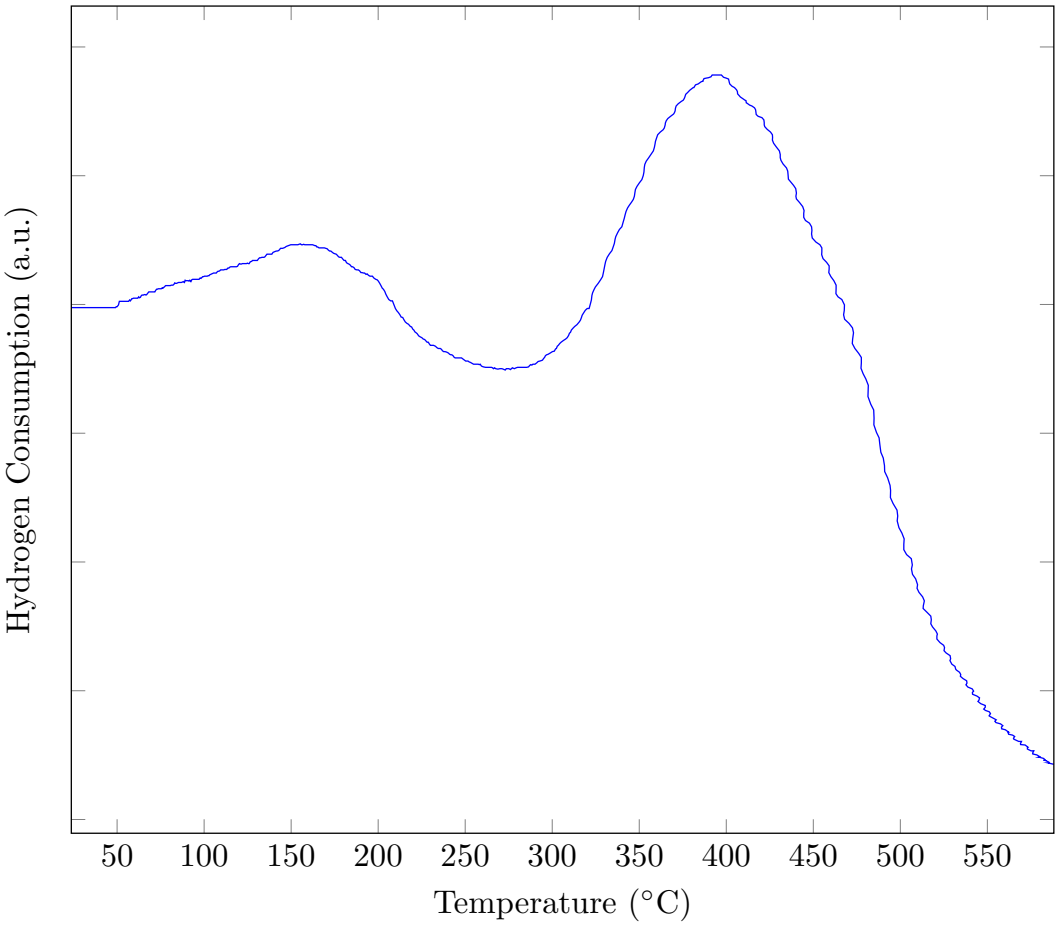

Figure 5.5: Temperature reduction profile for 4wt% Ag/TiO_2-Quantachrome Laboratory

Table 5.2: Temperature reduction profiles at various Ag wt % loadings

Ag Loading (wt %)	$T_{1\,max}$ (°C)	$T_{2\,max}$ (°C)	$T_{3\,max}$ (°C)	Ratio of Phase 1 : Phase 2	Average H_2 Consumption Phase (1&2) (μmoles)	Average H_2 Consumption Phase (3) (μmoles)
1	102	146	292	0.57	3.91	6.81
2	103	140*	341	0.35	4.50	13.0
3	102	146	292	0.56	7.88	13.7
4	114	140*	339	0.60	10.1	17.0
5	129*	153	328	0.70	11.6	16.5
6	108	140*	313	1.08	17.3	16.0
10	106	171	322	1.99	32.0	16.0
12	103	152	305	2.51	87.6	34.6

* shoulder exists instead of peak

Table 5.3: Amount of oxide reduced by TPR

Ag Loading	Total H_2 Consumption (μmol)	Mass of Ag_2O (g)	Mass of Ag (g)	Actual Ag Deposited (g)	Amt of Oxide Reduced	Ag Reduced %
2	17.45	0.004045	0.0038	0.0115	0.3277	33
3	21.55	0.004996	0.0047	0.0172	0.2698	27
4	21.45	0.004970	0.0046	0.0230	0.2013	20
5	27.13	0.006286	0.0059	0.0287	0.2037	20
6	28.10	0.006512	0.0061	0.0345	0.1759	18
10	33.31	0.007718	0.0072	0.0575	0.1251	13

* assuming 100 % Ag_2O

Sources of Error

Deviations in T_{max} maybe due to the temperature difference between the heating device and the sample temperature. To reduce lagging temperature the sample thermocouple was affixed directly outside the sample cell. A more accurate representative of the real sample temperature could be obtained by placing a thermocouple covered by a inert sheath in the adsorbent sample to monitor the reaction.

Also, errors may have arisen due to the TCD signal being out of sync with the timing of the heating device. The TCD signal was sampled at a rate of 5 Hz over a definite period of time. Thus, if the heating device/process controller moved too slowly or too quickly over a given period, the subsequent voltage to temperature conversions would be affected. Note that a 1°C deviation occurred in 6 seconds when operating at a temperature ramp of 10°C/min.

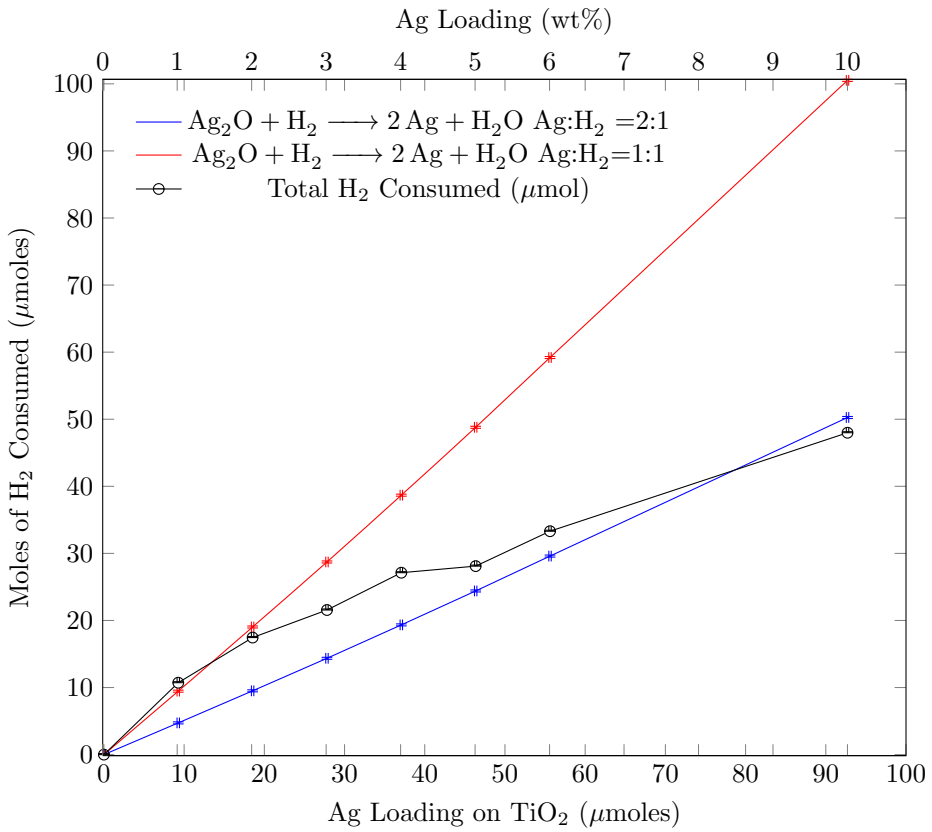

Figure 5.6: Temperature reduction number of moles of Ag Reduced assuming Ag^{+2} and Ag^{+1} species

Chapter 6

Silver-Titania Adsorbents: Discussion

The Center for Microfibrous Material Manufacturing (CM^3) developed silver based adsorbents for the ambient desulfurization of high sulfur fuels. Ag/TiO_2 has been shown useful for selective adsorption of sulfur heterocycles from complex fuel mixtures. Ag/TiO_2 adsorbent's utility involves simple and cost effective preparation, no hydro-processing, ambient operating conditions, and stable multi-cycle regeneration. 4 wt% Ag/TiO_2 has shown a remarkable adsorption of selectivity towards sulfur heterocycles such as benzothiophene and other dimethyl substituted compounds at ppb levels compared to other background fuel aromatics at up to 30% composition [22, 28]. As a result, a number of techniques have been used for characterizing this system. Transmission electron microscopy (TEM), electron paramagnetic resonance (EPR), X-ray diffraction (XRD), and oxygen chemisorption (OC) have been previously employed in an attempt to elucidate the surface behavior of this adsorbent [3, 22, 28, 29]. Silver atom dispersion and crystallite size are two crucial factors that influence capacity and selectivity of the adsorbent. Thus, it is important to employ techniques that give fundamental and uniform insight into this behavior. Unfortunately, each of the techniques noted above provides specific insight that is predicated by the biases, assumptions and sampling physics of the technique employed. As a result, inferential agreement has been limited from these studies and they generally do not conform with observed trends in heterocycle adsorption capacity versus Ag loading.

With regards to particle size and dispersion determinations, XRD did not provide useful information for *highly dispersed* Ag. The two main drawbacks of XRD particle size determination are that the average particle size is a volume weighted average (instead of a more appropriate surface weighted average) and the lower detection limit is reported to be for

crystallites that are $\gtrsim$ 5 nm [30–32]. TEM analysis is equally challenging as it is prone to various contrast issues and potential beam damage resulting from using a high surface area TiO_2 support (ca. 150 m^2/g). Also, TEM samples only a very small and selected fraction of the available crystallites and multi-atom agglomerations are not readily observable. Monodispersed silver atoms and multi-atom clusters are difficult and daunting targets for routine TEM analysis. EPR is dependent on the presence of certain oxidation states, e.g., Ag^0 and Ag^{2+}, while invisible to others such as Ag^{1+}. And while oxygen chemisorption is the most extensively used technique for determining the surface area weighted - average Ag crystallite size; the accuracy and utility of this technique depends severely on underlying assumptions regarding the: (i) conditions necessary to produce monolayer oxygen coverage, (ii) stoichiometry of the oxygen to surface atom ratio, (iii) insensitivity of the former on crystallite size, habit and surface plane(s) exposed, and (iv) inability to see those surface Ag atoms which do not undergo reversible re-dox processes at the conditions of the adsorption experiments. Monodispersed Ag^{1+} atoms and multi-atoms clusters which are strongly associated with TiO_2 surface defects have been inferred recently to be active sites for heterocycle adsorption based upon infrared adsorption spectra [108, 109] and corresponding 'DFT' calculations [110]. It is doubtful that these types of Ag atoms and clusters would be readily observable via the traditional characterization techniques of: XRD, EPR, TEM or OC. Therefore, there is a need for a more direct analysis technique that is capable of assessing the state of dispersion of Ag on high surface area TiO_2 supports.

XPS is well-suited for studying highly dispersed surface atoms, regardless of oxidation state, that are present in supported catalysts and adsorbents [44–53]. XPS also provides an assessment/indication of crystallite size that is strongly (and exponentially) weighted toward the surface atoms via the inelastic mean free path of the photoelectrons. In contrast to chemisorption, XPS can also detect metal and non-metals, as well as both reducible and irreducible species. Atoms on the surface and immediate subsurface will be seen regardless of oxidation state. Finally, XPS is able to simultaneously account for oxidation,

degree of dispersion, and nucleation/growth. Based on these studies a growth hypothesis was developed.

6.1 Development of Growth Hypothesis Model

The most common lattice plane for anatase TiO_2 is (101), followed by the (100), and (001) planes [111–114]. The (101) surface is also the most thermodynamically stable under clean conditions, while the (100) surface is thought to be more stable among oxygenated surfaces [115, 116], thus, the (101) surface was used as the basis for the schematic depiction. The introduction of silver ions into the surface of the TiO_2 enhances the sulfur heterocycle adsorption capacity as previously stated [4, 22]. The mechanism can be explained by the filling of point defects on the surface of the TiO_2 up to an optimal concentration, i.e. weight loading. The concentration of silver ions has a notable effect on the capacity of the TiO_2. Adsorption data demonstrated that varying metal loading of silver ions changed the capacity of sulfur heterocycle adsorption up to an optimal loading after which little or no increase in sulfur heterocycle adsorption capacity was achieved [22]. The introduction of metal ions could produce O vacancy or interstitial Ti^{4+} in TiO_2 [117]. However, due to the large ionic radius of silver compared to Ti^{4+}, it is unlikely that the silver ions would act as interstitial ions in the TiO_2 matrix. Thus, the point defect is depicted by an oxygen vacancy on the surface of the TiO_2.

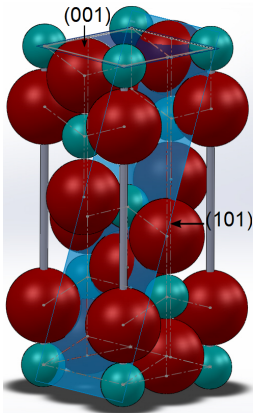

Figure 6.1: TiO_2 anatase unit cell showing the (001)(101) planes

The diagrams in Figure 6.2 are a representation of a model surface of the adsorbent at the various weight loadings that are consistent with the experimental results of the XPS. At the 2 and 4 wt% loadings it is believed that the Ag sites are of the same size but increase in occurrence as the weight loading of silver increases. This theory is due to the fact that 0, 2,

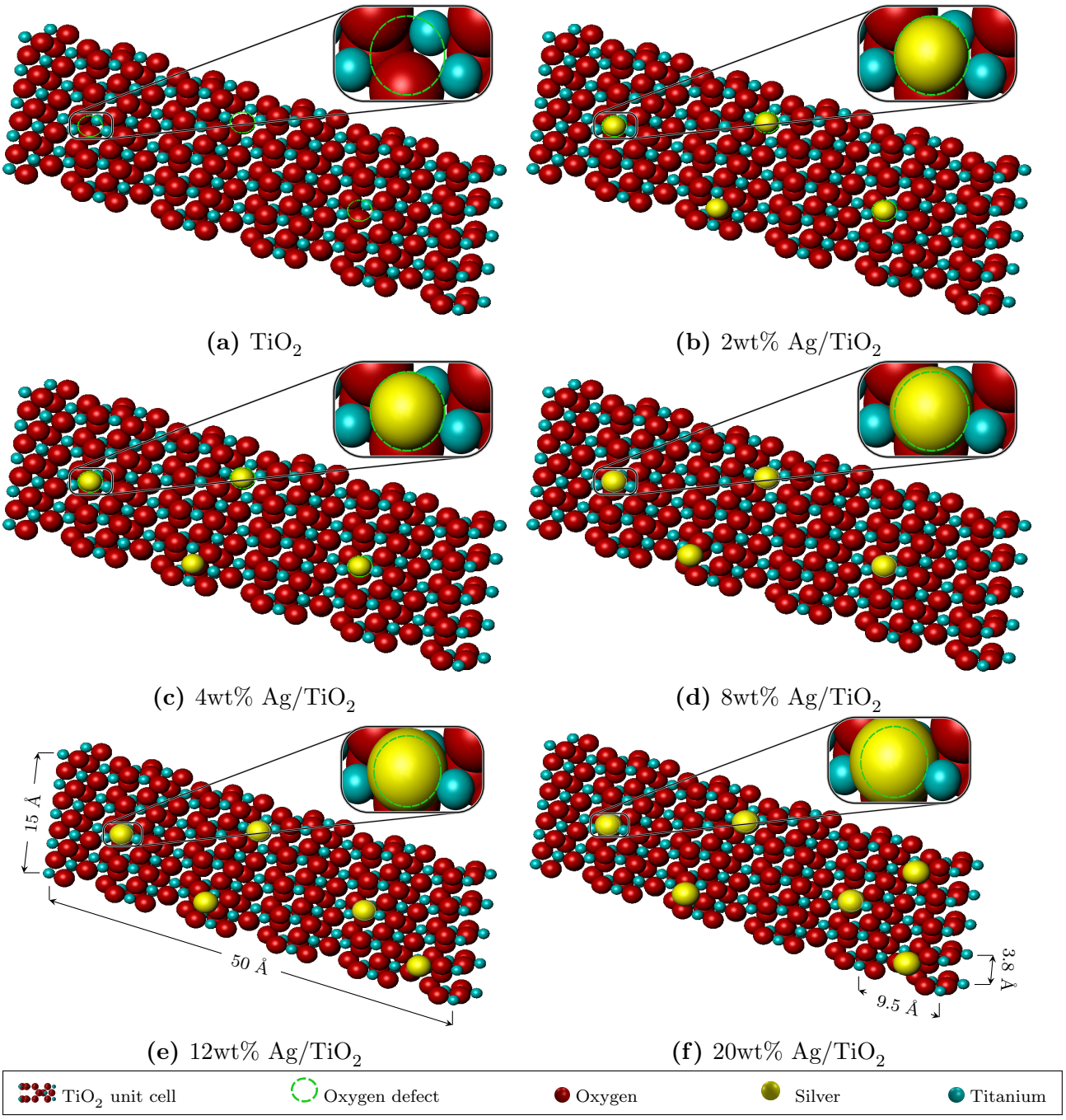

(a) TiO_2 **(b)** 2wt% Ag/TiO_2

(c) 4wt% Ag/TiO_2 **(d)** 8wt% Ag/TiO_2

(e) 12wt% Ag/TiO_2 **(f)** 20wt% Ag/TiO_2

Figure 6.2: Schematic showing the morphological configuration of Ag agglomerates with increasing loading on TiO_2

and 4 wt% loadings lie on the same line segment. At $\leq$ 4 wt% loading, the Ag crystallites occupy surface defects on the titanium surface and all the atoms are settled on the surface. It is theorized that all the surface defected on TiO_2 sites are populated at about the 4 wt% loading level and further increases in loading result in particle nucleation and growth. At 8 wt% loading, the silver coverage is about 0.28 ML (Figure 2.6), hence it can be assumed that silver atoms can still occupy the available surface on the TiO_2. However, there are no more defects available on the titanium sites that can hold the individual silver atoms strongly. At the 8, 12, and 20 wt% loadings the crystals grow progressively larger as revealed by the particle size estimations from the measured I_{Ag}/I_{Ti} intensity ratios.

6.2 Self Consistency Check of Ag Atom Balance versus Uniform Dispersion Behavior

An analysis was performed to test the credibility of the particle size distribution with regards to uniform behavior. The plot in Figure 6.3 is a calculation of the limits of particle size distribution based on the observed intensity XPS I_{Ag}/I_{Ti} diminution as well as the silver mass balance.

The number of the nucleation site is fixed by surface area, preparation and number of defects. This is believed to occur at the 4 wt% loading, thus 4 wt% loading is assumed to be the base number of available nucleation sites. The sizes of the particles at 8, 12 and 20 wt% were determined using experimental Ag/Ti intensity ratios. The atoms in the particles were determined based on a Ag^{1+} FCC unit cell on a volume basis (radius, r= 1.26 Å, lattice parameter a= 3.56 Å). The Ag unit cell was calculated using the volume of a cube with length = lattice parameter, a. The volume the particle was calculated using the volume of the sphere. Hemispherical particles would have increase the fraction of base sites Ag occupied on TiO_2 by a factor of 1/6 and cubic particle would have decreased that number by a factor of 2. The number of unit cells contained in each particle was derived and subsequently, the number of atoms was determined using 4 atoms/ FCC unit cell and 0.74 packing factor.

On the x-axis, at 0 there is no nucleation possible at the available sites, while at 1, all the sites are available for nucleation. However, all sites cannot uniformly gain additional atoms and satisfy the atom balance by occupying 100 % of the nucleation sites available. If all atoms were dispersed uniformly, there would be no diminution in signal because XPS can fully detect clusters of 3-5 atoms necessary for uniform distribution for 8–20 wt% loadings. Thus, it is hypothesized that only a fraction of the nuclei grew larger. At 8 wt% loading, the maximum fraction of sites available for nucleation is 0.5, assuming all sites uniformly gain 3 atoms (this is number of atoms determined to satisfy the XPS I_{Ag}/I_{Ti} intensity balance at this particular weight loading). Similarly, at 12 wt and 20 wt% loadings the maximum fraction of nucleation sites available are 0.15 and 0.12 respectively. The minimum number of atoms determined to satisfy the intensity balance at this particular weight loading at each nucleation site. Figure 6.3 clearly indicates the fact that uniform Ag behavior is not occurring, and that only a fraction of the crystallites grew to an appreciable amount.

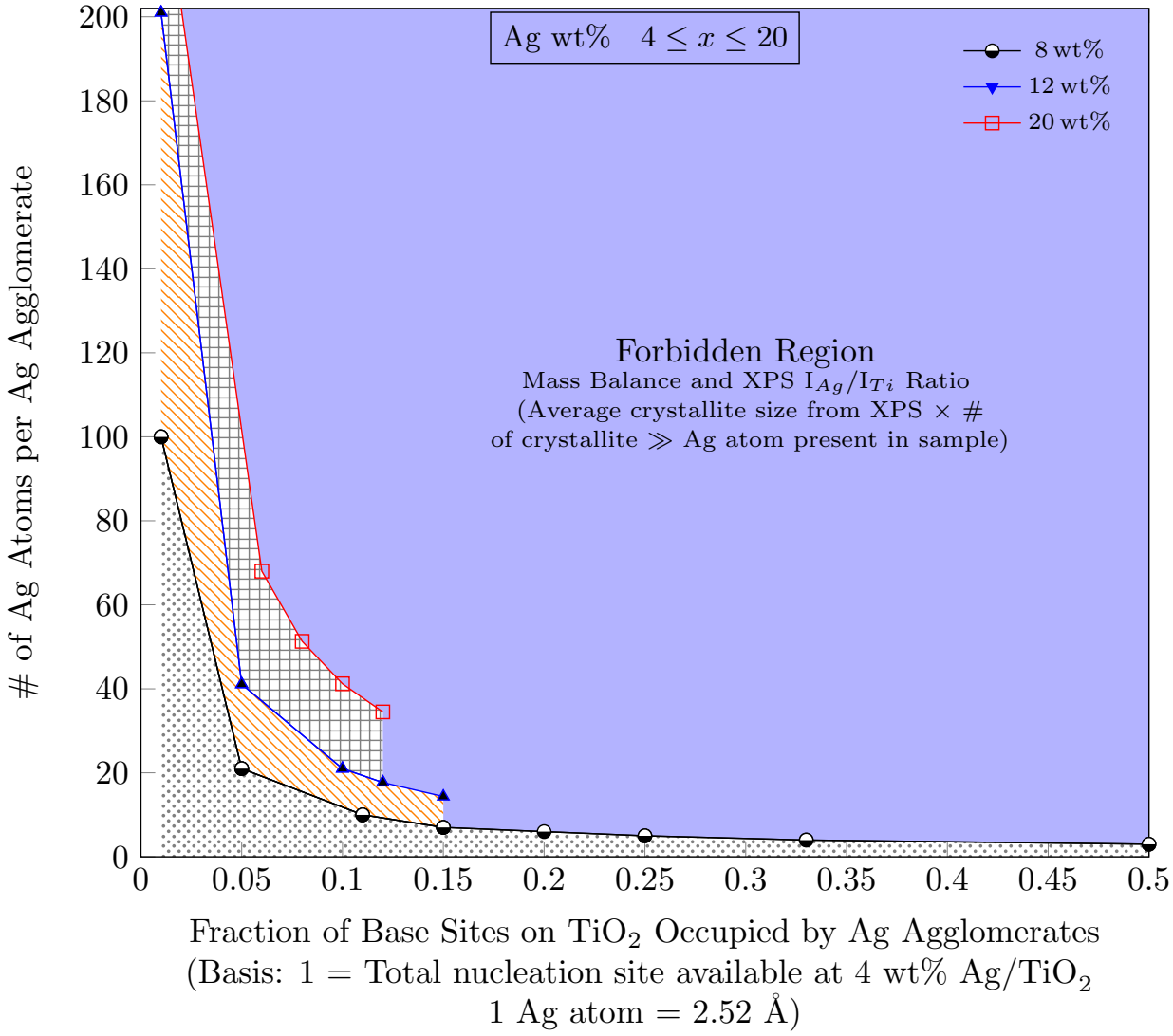

Figure 6.3: Fraction of Base Sites on TiO_2 Occupied by Ag Agglomerates

6.3 Sulfur Heterocyle Adsorption on 4 wt% Ag/TiO_2

Sulfur heterocycle adsorption capacities of different supports and metal loadings have been reported in past studies [4, 22, 109, 118–122]. A greater adsorption capacity for model fuel with benzothiophene (BT) than jet fuel, JP-5 was observed, this is due to competitive adsorption among all the compounds present in JP5 - sulfur compounds and non sulfur aromatic compounds. The sulfur heterocycle adsorption capacity of 4 wt% Ag/TiO_2 using benzothiophene (BT) (3500±10ppmw) in n-octane was reported as 41.7 mg of BT/g of sorbent. The native adsorption capacity of titania was 18.3 mg. The difference in sulfur adsorption capacity 23.4 mg was specifically due to the addition of Ag atoms to the titania substrate. Thus, at saturation, the Ag : BT ratio was approximately 2 Ag atoms to 1 BT molecule. Previous studies have shown 4 wt% Ag/TiO_2 to be a stable adsorbent for up to 10 regeneration cycles. 4 wt% Ag/TiO_2 does not leach during regeneration tests [4, 22, 121]

Table 6.1: Sulfur capacity of blank TiO_2 and 4 wt% Ag/TiO_2 using benzothiophene (3500± 10ppmw) in n-octane [1]

	Saturation Capacity (mg of BT/g of sorbent)
Blank TiO_2	18.3
4 wt% Ag/TiO_2	41.7
Difference	23.4

Chapter 7

Conclusion

Absorption studies were performed in an attempt to gain a better understanding of the discrepancies that exist between the previously reported average crystallite sizes for silver titania adsorbents using oxygen chemisorption and XPS. Oxygen chemisorption, the standard technique for determining average particle size and dispersion is predicated on strong assumptions that easily lead to a misrepresentation of surface characteristics. Although XPS is subjected to different constraints and assumptions, using Ag/Ti ratio is a credible indicator of the state of dispersion and average crystallite size of Ag in the silver titania system and possibly other systems containing silver. An atom balance versus intensity balance demonstrates a bimodal particle size distribution is a representation of the sample and is important to correlate the activity of supported silver adsorbents and catalysts to their structure–activity performance. Accounting for the native uptake of nitrated titania surface and using a Ag/O stoichiometric ratio of 2 for the polycrystalline of the silver titania system surface gave a more accurate representation of the particle size and average crystallite sizes. Thus it is recommended that XPS is more widely used for the aforementioned purposes.

The model predicting the particle growth behavior of silver on polycrystalline titania was improved showing estimates of the upper ranges of bimodal particle size distribution behavior. The latter behavior not being readily observable from techniques which assume uniform or average population behavior. Also notable is the observed heterocycle adsorption trends versus Ag loading agree closely with the dispersion and nucleation trends deduced from XPS-Ag/Ti intensity ratios. This study also showed that oxygen chemisorption appears to be surface confined.

7.1 Contribution to Engineering Science

These studies promote engineering development in surface characterization, catalysis, desulfurization, fuel processing for fuel cells and ultimately power generation. An awareness of the analysis of material surfaces involving the utility of XPS outside its common place use has been extended. The characteristics of Ag/TiO_2 system have been identified using a multi-technique approach. The biases and varying perspectives of oxygen chemisorption and XPS have been examined in their application to the Ag/TiO_2 system and a bimodal particle size distribution has arisen to be a true representation of the sample.

S-adsorption mechanism of Ag/TiO_2 system requires a combination of a sequence of events:

- Support — TiO_2 anatase is defected and consists of surface hydroxyl groups
- Addition of silver ion dopants– Optimization occurs when all the defects on the surface of the TiO_2 are filled by Ag^{1+} ions. Hydroxyl groups are mobilized and enhanced by the addition of highly dispersed hydrophilic Ag^{1+} ions.
- Ag/TiO_2 interaction with S-heterocycles–Interaction with hydroxyl groups promote pi complexation [123] or interaction facilitate a dissociative reaction (based on TPD study [124]). Different sulfur species are both reduced and completely oxidized.
- Fourfold coordination for Ag and S requires surface O^{2-} and OH^{-} interaction based on equivalent OH (bridging O) interaction with pi electrons and non equivalent OH (TiO_2 interaction with pi electrons).

Chapter 8

Recommendations for Future Work

The following experiments are proposed to resolve the disparities that arose during these studies:

- Perform XPS and oxygen chemisorption on the same sample batch
- Investigate the possibility of a bimodal distribution using oxygen chemisorption
- Perform O_2/H_2 titration on adsorbent
- Investigate the 2.5 oxygen to silver chemisorption ratio

Temperature programmed studies are also proposed to investigate the release characteristics of sulfur containing polycyclic aromatic hydrocarbons (PAHs). The goal of this study is to determine why specific PAH compounds preferentially bind to the Ag/TiO_2 adsorbent, the degree of binding, and the geometry influencing binding.

8.1 Ag/TiO_2 Acid Site Evaluation by Temperature-Programmed Desorption of Probe Molecules

In this study, the exploration of the desorption kinetics, surface reaction mechanisms, nature of the surface intermediates and surface acidity using temperature programed analysis is proposed. Investigate the acidity of Ag/TiO_2 adsorbents by TPD/TPRS using probe molecules such as ammonia and pyridine that provide selective interaction with the surface sites. Ammonia can be used to indicate strong and weak Brønsted and Lewis sites while pyridine can be used to discern the nature - Brønsted or Lewis, of the acid sites. [125–128].

The adsorbate will be monitored through a mass spectrometer. The desorption spectrum is a graph of counts per second as a function of temperature. Acidity strength is typically indicated by the temperature of the peak maxima of the desorption spectra. More detailed information can be obtained by evaluating the energies of desorption. However, difficulties lie with poor spectral resolution, diffusion limitations, and comparison with analogous adsorbate–adsorbent systems.

A series of experiments are proposed where the effects of the nature of the probe molecules will be monitored with the systematic variation of Ag/TiO_2 adsorbents with weight loading ranging from 0–20 wt%. Additionally, if time permits, experiments evaluating the temperature-programmed XPS of the chemisorption assumptions and conditions will be performed. This would provide a better understanding of oxygen chemisorption when used with silver particles.

8.2 Investigation of the Adsorption Process and Assessment of the Removal Pathway

In TPD, the ion intensity is proportional to the rate of desorption (dh/dt) and the total area under the thermogram curve is proportional to the amount originally adsorbed. TPD–MS results can provide qualitative information relating the adsorbed species and their desorption rates, which will be useful in optimizing the adsorbent regeneration process. Using the TPD-MS thermogram, the desorbing molecules can be determined by their mass and mass spectral fragmentation patterns. Ion intensities for selected mass-to-charge ratios (m/z) are identified and assigned to desorbing species. Special identification is achieved through comparison with known standards.

The introduction of selective refractory heterocyclic species, such as thiophene and benzothiophene in TPD/TPRS will enable the assessment specificity of various heterocyclic compounds. Since it is known that the surface of the Ag strongly influences the sorbent's affinity for the refractory heterocyclic compounds. Studying the elution pattern of such refactory compounds may lead to the understanding of the desorption pathway and possibly an optimization of the regeneration pathway of Ag/TiO_2 adsorbents. It is reported that Ag forms step edges at which the sulfur binds on Ag surfaces [129, 130]. Thus, it is likely that it is the structure of the edges that facilitate the 'lock' for these big refractory compounds.

8.3 Investigation of the structural role of Ag in TiO_2 support and its paramagnetic behavior by EPR

Previous work using EPR, revealed that only ~ 0.1 % of the total Ag was present as Ag^{2+} on the 4 wt% Ag/TiO_2 sorbent [28]. The shift towards lower B.E in the XPS spectra of the Ag 3d peaks from the 4 wt% to the 20 wt% loading of Ag/TiO_2 (see figure 2.4) prompted complementary investigation by EPR. Specifically, the EPR signal for nanoparticles of metallic Ag, evident at about 3250 G and 3350 G was investigated [131].

The 2, 4, 8, 20 wt% loadings of Ag/TiO_2 were analyzed in an attempt to resolve the EPR line for Ag^0 and the Ag^{2+} species. The results were inconclusive with regards to the presence of the Ag^0 line. The EPR signal for the Ag^{2+} species was most easily identified in the 4 wt% loading. This result correlated with other findings [22], which lead to the conclusion that 4 wt% Ag/TiO_2 has special properties that enhances its capacity for sulfur removal. In the 8 and 20 wt% loadings the Ag line could have be present in the 3250 - 3400 G region, but the positions of the line were obscured by other absorptions present in the sample (see Figure 8.1). Specifically, the titanium EPR line, which has been reported to be broadened in this region by the presence of NO bound to the bulk titania [3, 132]. There exists a small concentration of NO bound to bulk TiO_2 in the Ag/TiO_2 sorbent [3]. Resolution of the Ag signal in the Ag/titania sorbent was difficult because the EPR signal due to trapped nitrate and Ag/titania sorbent are identical, and thus could not be individually identified.

The identification of the Ag^0 species should be investigated by implementing a stepwise approach. The following three parts are proposed: Firstly, identify and isolate the Ag^0 on a different support. Stabilized silver atoms were obtained at 77 K by irradiating alkali halide crystals containing silver ions [133]. Next, identify the structural configuration which is energetically favorable for the existence of stable Ag on the TiO_2 support by creating paramagnetic centers. EPR spectral lines should be present at about 3000 G to 3600 G due to Ag^0 [134–136]. Thirdly, investigate the existence of Ag^0 at 473 K signal that was

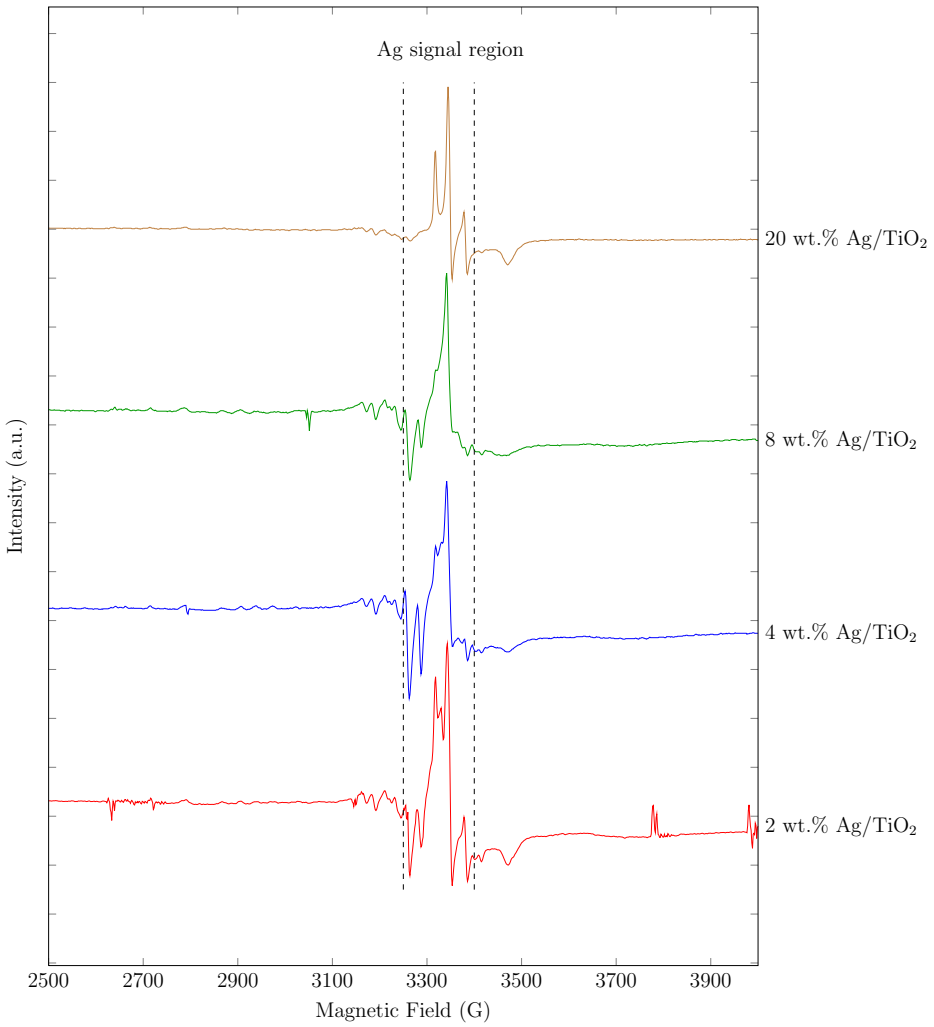

Figure 8.1: EPR spectra of the Ag/TiO_2 at 77 K

reported in Wang and Weh [136], which should be absent at room temperature due to sample exposure to air see, Figure 8.2.

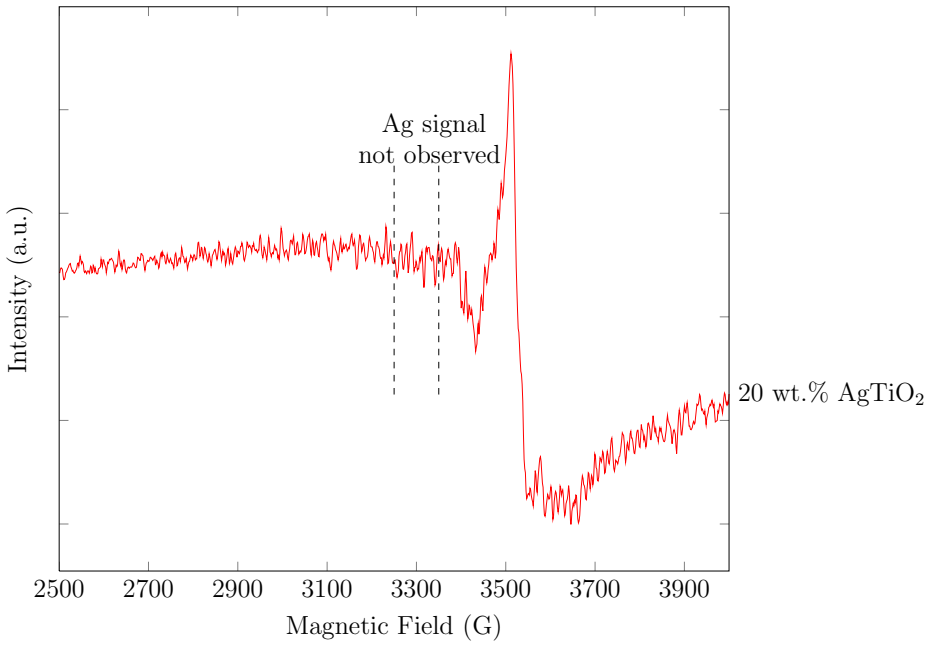

Figure 8.2: EPR spectra of the Ag/TiO_2 at 298 K

Since it is believed that mostly Ag^{+1} is present at low loadings, Ag at loading of 20 wt% or more should be investigated to confirm the presence of Ag metal. Metallic silver was detected by XRD at 20 wt% loadings of Ag, however it was not quantifiable due to the small amount and the uncertainty that this introduces. An EPR investigation into the reduced samples could also be performed to complement TPR studies.

8.4 Additional XPS characterization.

Perform XPS investigation on the adsorbent system Ag/TiO_2 using a more sensitive system than the non-monochromated LHS-10. XPS has become even more powerful with new technological advancements: higher counting rates, more sensitive detection limits, narrower FWHM, and greater signal-to noise ratios. These new advances have enabled acquisition of more fundamental surface chemical information. Thus, more information can be extracted by

the technique since limitations encountered previously were due to the current XPS system and the technique.

Examination of the Ag Auger energy levels to distinguish the factors such as static relaxation term influencing chemical shifts in the Ag/TiO_2 adsorbent. Comparison of the Auger energy shifts and binding energy shift can lead to the identification of the Ag chemical environment. Also, XPS can be used as a complementary technique to TPD/TPRS to study surface acidity of Ag/TiO_2. This technique has been used to study the adsorption of probe molecules such as: benzene, pyridine, and pyrrole in literature [87, 137, 138]. Specifically, to perform alkali treatment to modify acid-base properties to investigate surface acidity.

TPD/TPRS was used to investigate the release characteristics of sulfur containing polycyclic aromatic hydrocarbons (PAHs). 4wt % Ag-TiO_2 sorbents were dosed with model fuels containing representative PAHS compounds, such as: Thiophene (T), Benzothiophene (BT) and Dibenzothiophene (DBT). Real time desorption spectra were obtained outlining the thermal desorption profile of the sorbent. These profiles show that the PAHs do not desorb molecularly, they fragment into various compounds which are eluted at different peak temperatures of desorption. The goal of this study is to determine why specific PAH compounds preferentially bind to the Ag-TiO_2 adsorbent, the degree of binding, and the geometry influencing binding.

8.5 Investigation into the Sintering Behavior of Ag/TiO_2 Adsorbents

Sintering, is the process by which larger particles are formed through chemical bonding under the influence of temperature, pressure, or both. The sintering process is complex, different factors such as driving forces and material transport system need to be considered. Factors affecting sintering depend both on the material characteristics and processing parameters. The traditional approach will be employed to develop a simple sintering method by varying one factor and holding all other factors constant.

The Ag/TiO_2 adsorbents which are prepared by incipient wetness impregnation will be subjected to different sintering conditions. The aim of this study will be to elucidate the sintering behavior of the Ag/TiO_2. This, in an effort to understand densification and the effect of sintering on the silver particle size. Insights into the sintering behavior will be integral in controlling particle size.

Currently, it is believed that the surface defects of TiO_2 and the particle size of silver are interrelated and ultimately responsible for the sulfur capacity of Ag/TiO_2 adsorbents. Silver is mono-dispersed up to the 4 wt% loading baseline. Isolated silver atoms occupy the surface defects until they are filled, after which particle growth begins. Thus, subsequent beneficial steps would be to :

- Develop a more defected surface (currently being by investigated another member of CM^3)
- Find the optimal particle size that can fill these defects. Limit crystal size distribution to a very narrow range; which, considering anecdotal sulfur capacity absorption studies, is optimal around 4 wt% loading of silver particles. This would lead to the need to develop a process to control the variable in the synthesis of Ag/TiO_2 adsorbents. This variable may be determined by performing sintering studies focusing on the two processing factors - temperature and sintering time.

The investigation will show the nucleation and growth of the mobile silver particles with respect to sintering temperature and time. Ag/TiO_2 samples will be annealed at various temperatures for example 400, 450, 500 °C, etc. for various lengths of time 15, 30, 60 minutes, etc. Subsequent characterization will be performed by XRD, optical microscopy, SEM, EDS, EPR, and XPS. Informative plots such as the I_{Ag}/I_{TiO_2} as a function of the annealing temperature and time or Ag particle size as a function of sintering time should provide insight into the behavior of silver. If applicable, the lattice constants will be determined from XRD. Variations in the lattice constants indicate changes in the cation distribution in the interstitial sites.

Difficulties may arise because the number of runs increase significantly with the number of experimental variables. However, by limiting the range of experimental settings of temperature and time based on the current sample preparation process, there will be a predetermined end to these experiments. The temperature range will be between 300–550 °C, in increments of 50 °C, and the time range will be 15 and 30 minutes.

Bibliography

[1] A. S. Hussain, "Laboratory notebook." 2013.

[2] B.Tatarchuk, H. Yang, and S. Nair, "Silver-Based Sorbents," April 2008. US 2008/0283446 A1.

[3] A. Samokhvalov, E. C. Duin, S. Nair, M. Bowman, Z. Davis, and B. J. Tatarchuk, "Study of the Surface Chemical Reactions of Thiophene with Ag/Titania by the Complementary Temperature-Programmed Electron Spin Resonance, Temperature-Programmed Desorption, and X-ray Photoelectron Spectroscopy: Adsorption, Desorption, and Sorbent Regeneration Mechanisms," *The Journal of Physical Chemistry C*, vol. 114, no. 9, pp. 4075–4085, 2010.

[4] S. Nair and B. Tatarchuk, "Characteristics of Sulfur Removal by Silver-Titania Adsorbents at Ambient Conditions," *Adsorption*, vol. 17, pp. 663–673, 2011.

[5] Z. Davis, "A Multi-Technique Comparative Evaluation of Ag Dispersion on Polycrystalline TiO_2," Master's thesis, Auburn University, 2012.

[6] K. Segawa, K. Takahashi, and S. Satoh, "Development of New catalysts for Deep Hydrodesulfurization of Gas Oil," *Catalysis Today*, vol. 63, pp. 123 – 131, 2000.

[7] S. Velu, X. Ma, and C. Song, "Selective Adsorption for Removing Sulfur from Jet Fuel over Zeolite-Based Adsorbents," *Industrial & Engineering Chemistry Research*, vol. 42, no. 21, pp. 5293–5304, 2003.

[8] S. K. Bej, S. K. Maity, and U. T. Turaga, "Search for an Efficient 4,6-DMDBT Hydrodesulfurization Catalyst:A Review of Recent Studies," *Energy & Fuels*, vol. 18, no. 5, pp. 1227–1237, 2004.

[9] A. J. Hernandez-Maldonado and R. T. Yang, "Desulfurization of Liquid Fuels by Adsorption via Complexation with Cu(I)Y and AgY Zeolites," *Industrial & Engineering Chemistry Research*, vol. 42, no. 1, pp. 123–129, 2003.

[10] A. J. Hernandez-Maldonaldo and R. Yang, "Desulfurization of Transportation Fuels by Adsorption," *Catalysis Reviews*, vol. 46, no. 2, pp. 111–150, 2004.

[11] S. Velu, X. Ma, C. Song, M. Namazian, S. Sethuraman, and G. Venkataraman, "Desulfurization of JP-8 Jet Fuel by Selective Adsorption over a Ni-based Adsorbent for Micro Solid Oxide Fuel Cells," *Energy & Fuels*, vol. 19, pp. 1116–1125, 2005.

[12] X. Ma, S. Velu, J. H. Kim, and C. Song, "Deep Desulfurization of Gasoline by Selective Adsorption over Solid Adsorbents and Impact of Analytical Methods on ppm-level Sulfur Quantification for Fuel Cell Applications," *Applied Catalysis B: Environmental*, vol. 56, no. 1-2, pp. 137 – 147, 2005.

[13] J. H. Kim, X. Ma, A. Zhou, and C. Song, "Ultra-deep Desulfurization and Denitrogenation of Diesel Fuel by Selective Adsorption over Three Different Adsorbents: A Study on Adsorptive Selectivity and Mechanism," *Catalysis Today*, vol. 111, no. 1-2, pp. 74 – 83, 2006.

[14] P. T. Vasudevana and J. L. G. Fierro, "A Review of Deep Hydrodesulfurization Catalysis," *Catalysis Reviews: Science and Engineering*, vol. 38, pp. 161–188, May 1996.

[15] X. Ma, K. Sakanishi, and I. Mochida, "Hydrodesulfurization Reactivities of Various Sulfur Compounds in Vacuum Gas Oil," *Industrial & Engineering Chemistry Research*, vol. 35, no. 8, pp. 2487–2494, 1996.

[16] G. Khare and D. Engelbert, "Desulfurization and Novel Sorbent for Same," 2004.

[17] A. Pricem, J. Gislason, G. Dodwell, R. Morton, and G. Parks, "Desulfurization of Hydrocarbon Stream using Novel Compositions Containing Manganese Oxide.," 2006.

[18] E. Simon, W. Morton, R. Schmidt, J. Gislason, and B. Welch, "Reduced-valence Metal-promoted Niobium Oxide and Tantalum Oxide as Petroleum Desulfurization Sorbents," 2004.

[19] J. Gislason, R. Schmidt, M. Welch, D. Simon, and R. Morton, "Method for Reducing the amount of High Molecular Weight Organic Sulfur picked-up by Hydrocarbon Streams Transported through a Pipeline," 2005.

[20] X. Ma, M. Sprague, and C. Song, "Deep Desulfurization of Gasoline by Selective Adsorption over Nickel-Based Adsorbent for Fuel Cell Applications," *Industrial & Engineering Chemistry Research*, vol. 44, no. 15, pp. 5768–5775, 2005.

[21] B. Tatarchuck, H. Yang, and P. Dhage, "Doped Supported Zinc Oxide Sorbents for Regenerable Desulfurization Applications," 2008.

[22] S. Nair and B. J. Tatarchuk, "Supported Silver Adsorbents for Selective Removal of Sulfur Species from Hydrocarbon Fuels," *Fuel*, vol. 89, no. 11, pp. 3218–3225, 2010.

[23] A. Takahashi, R. T. Yang, C. L. Munson, and D. Chinn, "Influence of Ag Content and H2S Exposure on 1,3-Butadiene/1-Butene Adsorption by Ag Ion-Exchanged Y-Zeolites (Ag-Y)," *Industrial & Engineering Chemistry Research*, vol. 40, no. 18, pp. 3979–3988, 2001.

[24] S. Satokawa, Y. Kobayashi, and H. Fujiki, "Adsorptive Removal of Dimethylsulfide and t-Butylmercaptan from Pipeline Natural Gas Fuel on Ag Zeolites under Ambient Conditions," *Applied Catalysis B: Environmental*, vol. 56, no. 12, pp. 51 – 56, 2005.

[25] S. Velu, C. Song, M. H. Engelhard, and Y.-H. Chin, "Adsorptive Removal of Organic Sulfur Compounds from Jet Fuel over K-Exchanged NiY Zeolites Prepared by Impregnation and Ion Exchange," *Industrial & Engineering Chemistry Research*, vol. 44, no. 15, pp. 5740–5749, 2005.

[26] H. Yang, R. Sothen, D. R. Cahela, and B. J. Tatarchuk, "Breakthrough Characteristics of Reformate Desulfurization Using ZnO Sorbents for Logistic Fuel Cell Power Systems," *Industrial & Engineering Chemistry Research*, vol. 47, no. 24, pp. 10064–10070, 2008.

[27] P. Dhage, A. Samokhvalov, D. Repala, E. C. Duin, M. Bowman, and B. J. Tatarchuk, "Copper-Promoted ZnO/SiO_2 Regenerable Sorbents for the Room Temperature Removal of H_2S from Reformate Gas Streams," *Industrial & Engineering Chemistry Research*, vol. 49, no. 18, pp. 8388–8396, 2010.

[28] A. Samokhvalov, S. Nair, E. C. Duin, and B. J. Tatarchuk, "Surface Characterization of Ag/Titania Adsorbents," *Applied Surface Science*, vol. 256, no. 11, pp. 3647–3652, 2010.

[29] A. Samokhvalov, E. C. Duin, S. Nair, and B. J. Tatarchuk, "An in situ Temperature-Programmed XPS Study of the Surface Chemical Reactions of Thiophene with Ag/Titania," *Surface and Interface Analysis*, vol. 42, no. 9, pp. 1476–1482, 2010.

[30] J. Angevine, W. N.Delgass, and J. C.Vartuli, "Dispersion and Uniformity of Supported Catalyst by X-ray Photoelectron Spectroscopy," *Proceedings of the 6th International Congress on Catalysis*, vol. 2, pp. 611–620, 1976.

[31] S. C. Fung, "Application of XPS to the Determination of the Size of Supported Particles in a Catalyst–Model Development and its Application to Describe the Sintering Behavior of a Silica-Supported Pt Film," *Journal of Catalysis*, vol. 58, no. 3, pp. 454–469, 1979.

[32] D. G. Mustard and C. H. Bartholomew, "Determination of Metal Crystallite Size and Morphology in Supported Nickel Catalysts," *Journal of Catalysis*, vol. 67, no. 1, pp. 186–206, 1981.

[33] M. Treacy and A. Howie, "Contrast Effects in the Transmission Electron Microscopy of Supported Crystalline Catalyst Particles," *Journal of Catalysis*, vol. 63, no. 1, pp. 265–269, 1980.

[34] J. Sanders and K. Pratt, "The Relationship of Structure and Activity of NiMo Sulfides to Composition of the Precursor Oxides," *Journal of Catalysis*, vol. 67, no. 2, pp. 331–347, 1981.

[35] T. E. Whyte, "Metal Particle Size Determination of Supported Metal Catalysts," *Catalysis Reviews*, vol. 8, no. 1, pp. 117–134, 1974.

[36] J. R. Anderson, *Structure of Metallic Catalysts*. Academic Press Inc, 1975.

[37] S. Seyedmonir, D. E. Strohmayer, G. L. Geoffroy, M. Vannice, H. W. Young, and J. W. Linowski, "Characterization of Supported Silver Catalysts: I. Adsorption of O_2, H_2, N_2O, and the H_2-Titration of Adsorbed Oxygen on Well-Dispersed Ag on TiO_2," *Journal of Catalysis*, vol. 87, no. 2, pp. 424–436, 1984.

[38] D. E. Strohmayer, G. L. Geoffroy, and M. A. Vannice, "Measurement of Silver Surface area by the H_2 Titration of Chemisorbed Oxygen," *Applied Catalysisreporte*, vol. 7, no. 2, pp. 189–198, 1983.

[39] J. Scholten, J. Konvalinka, and F. Beekman, "Reaction of Nitrous Oxide and Oxygen with Silver Surfaces, and Application to the Determination of Free-Silver Surface Areas of Catalysts," *Journal of Catalysis*, vol. 28, no. 2, pp. 209–220, 1973.

[40] K. M. Kholyavenko, M. Y. Rubanik, and N. Chernukhina, "Determination of the Surface Area of Silver Deposited on a Carrier by Chemisorption," *Kinetika i Kataliza (Kinectics and Catalysis)*, vol. 5, no. 3, pp. 505–512, 1964.

[41] A. W. Czanderna, "The Adsorption of Oxygen on Silver," *The Journal of Physical Chemistry*, vol. 68, no. 10, pp. 2765–2771, 1964.

[42] M. Barteau and R. Madix, *The Surface Reactivity of Silver: Oxidation Reactions in: The Chemical Physics of Solid Surfaces and Heterogeneous Catalysis*, ch. 4, pp. 95–142. Elsevier, 1982.

[43] B. Kip, F. Duivenvoorden, D. Koningsberger, and R. Prins, "Determination of Metal Particle Size of Highly Dispersed Rh, Ir, and Pt Catalysts by Hydrogen Chemisorption and EXAFS," *Journal of Catalysis*, vol. 105, no. 1, pp. 26–38, 1987.

[44] J. S. Brinen, "Applications of ESCA to Industrial Chemistry," *Journal of Electron Spectroscopy and Related Phenomena*, vol. 5, no. 1, pp. 377–400, 1974.

[45] L. Scharpen, "The Dispersion of Platinum on Silica-Correlation of ESCA and Gas Adsorption Data," *Journal of Electron Spectroscopy and Related Phenomena*, vol. 5, no. 1, pp. 369–376, 1974.

[46] D. Briggs, "ESCA and Metal Crystallite Size/Dispersion in Catalysts," *Journal of Electron Spectroscopy and Related Phenomena*, vol. 9, no. 5, pp. 487–491, 1976.

[47] R. Shalvoy and P. Reucroft, "Quantitative Analysis of ESCA Signal Intensifies from Coprecipitated Nickel on Alumina Catalysts," *Journal of Electron Spectroscopy and Related Phenomena*, vol. 12, no. 3, pp. 351–356, 1977.

[48] M. Houalla and B. Delmon, "Use of XPS to Detect Variations in Dispersion of Impregnated and Ion-exchanged NiO/SiO_2 Systems," *Surface and Interface Analysis*, vol. 3, no. 3, pp. 103–105, 1981.

[49] C. Defosse, M. Houalla, A. Lycourghiotis, and F. Delannay, "Joint Use of X-Ray Photoelectron Spectroscopy and Analytical Electron Microscopy in the Investigation of Cobalt and Nickel Oxide Supported on Na-Doped Alumina," in *New Horizons in Catalysis Proceedings of the 7th International Congress on Catalysis* (T. Seivama and K. Tanabe, eds.), vol. 7, Part A of *Studies in Surface Science and Catalysis*, pp. 108–121, Elsevier, 1981.

[50] Z. Liu, Z. Lin, H. Fan, F. Li, Q. Bao, and S. Zhang, "Dispersion of V_2O_5 Supported on a TiO_2 Surface by X-Ray Photoelectron Spectroscopy," *Applied Physics A: Materials Science & Processing*, vol. 45, pp. 159–164, 1988.

[51] V. D. Castro, C. Furlani, M. Gargano, N. Ravasio, and M. Rossi, "XPS Study of Copper Dispersion in CuO/Al_2O_3 Catalysts," *Journal of Electron Spectroscopy and Related Phenomena*, vol. 52, pp. 415–422, 1990.

[52] S. Kaliaguine, "Application of Surface Science Techniques in the Field of Zeolitic Materials," in *Recent Advances and New Horizons in Zeolite Science and Technology* (S. W. H. Chon and S.-E. Park, eds.), vol. 102 of *Studies in Surface Science and Catalysis*, pp. 191–230, Elsevier, 1996.

[53] B. M. Reddy, B. Chowdhury, E. P. Reddy, and A. Fernndez, "An XPS Study of Dispersion and Chemical State of MoO_3 on Al_2O_3-TiO_2 Binary Oxide Support," *Applied Catalysis A: General*, vol. 213, no. 2, pp. 279–288, 2001.

[54] J. Brinen, J. Schmitt, W. Doughman, P. Achorn, L. Siegel, and W. Delgass, "X-ray Photoelectron Spectroscopy Studies of the Rhodium on Charcoal Catalyst: II. Dispersion as a Function of Reduction," *Journal of Catalysis*, vol. 40, no. 3, pp. 295–300, 1975.

[55] S. Kaliaguine, A. Adnot, and G. Lemay, "A Model for the Quantitative Analysis of ESCA Intensity Ratios for Supported Catalysts with Partial Surface Segregation," *The Journal of Physical Chemistry*, vol. 91, no. 11, pp. 2886–2890, 1986.

[56] S. Davis, "Particle Size Information from Dispersed Phase Photoemission Intensity Ratios," *Journal of Catalysis*, vol. 117, no. 2, pp. 432–446, 1989.

[57] S. Kaliaguine, A. Adnot, G. Lemay, and L. Rodrigo, "On the Quantitative Analysis of XPS Intensity Data for Supported Catalysts with Partial Surface Segregation," *Journal of Catalysis*, vol. 118, no. 1, pp. 275–279, 1989.

[58] E. Voogt, A. Mens, O. Gijzeman, and J. Geus, "XPS Analysis of Palladium Oxide Layers and Particles," *Surface Science*, vol. 350, no. 13, pp. 21–31, 1996.

[59] M. A. Wahab, *Solid State Physics: Structure and Properties of Materials*. Alpha Science International Ltd, 2nd ed., 2005.

[60] C. Brooks and G. Christopher, "Measurement of the State of Metal Dispersion on Supported Nickel Catalysts by Gas Chemisorption," *Journal of Catalysis*, vol. 10, no. 3, pp. 211–223, 1968.

[61] B. G. Linsen, ed., *Physical and Chemical Aspects of Adsorbents and Catalysts : Dedicated to J. H. de Boer on the Occasion of His Retirement from the Technological University, Delft, the Netherlands*. Academic Press, 1970.

[62] J. Regalbuto, T. Fleisch, and E. Wolf, "An Integrated Study of $Pt/WO_3/SiO_2$ Catalysts for the NO-CO Reaction: I. Catalyst Characterization by XRD, Chemisorption, and XPS," *Journal of Catalysis*, vol. 107, no. 1, pp. 114–128, 1987.

[63] D. Farin and D. Avnir, "Crystallite Size Effects in Chemisorption on Dispersed Metals," *Journal of Catalysis*, vol. 120, no. 1, pp. 55 – 67, 1989.

[64] R. Wojcieszak, M. J. Genet, P. Eloy, P. Ruiz, and E. M. Gaigneaux, "Determination of the Size of Supported Pd Nanoparticles by X-ray Photoelectron Spectroscopy. Comparison with X-ray Diffraction, Transmission Electron Microscopy, and H_2 Chemisorption Methods," *The Journal of Physical Chemistry C*, vol. 114, no. 39, pp. 16677–16684, 2010.

[65] J. Watts, "Surface Analysis — X-Ray Photoelectron Spectroscopy," in *Encyclopedia of Analytical Science* (P. Worsfold, A. Townshend, and C. Poole, eds.), vol. 8, pp. 5047–5058, Oxford: Elsevier, 1st ed., 1995.

[66] J. E. Fulghum, "Recent Developments in High Energy and Spatial Resolution Analysis of Polymers by XPS," *Journal of Electron Spectroscopy and Related Phenomena*, vol. 100, no. 13, pp. 331–355, 1999.

[67] S. Tougaard, "Surface Analysis — X-Ray Photoelectron Spectroscopy," in *Encyclopedia of Analytical Science* (P. Worsfold, A. Townshend, , and C. Poole, eds.), pp. 446–456, Oxford: Academic Press, 2nd ed., 2005.

[68] J. Walton and N. Fairley, "Characterisation of the Kratos Axis Ultra with Spherical Mirror Analyser for XPS Imaging," *Surface and Interface Analysis*, vol. 38, no. 8, pp. 1230–1235, 2006.

[69] J. I. Langford and A. J. C. Wilson, "Scherrer after Sixty Years: A Survey and Some New Results in the Determination of Crystallite Size," *Journal of Applied Crystallography*, vol. 11, pp. 102–113, Apr 1978.

[70] C. Suryanarayana and M. G. Norton, *X-ray Diffraction: A Practical Approach*. Springer, 1st ed., 1998.

[71] B. Cullity and S. Stock, *Elements of X-Ray Diffraction*. Prentice Hall, 3rd ed., 2001.

[72] P. Georgopoulos and J. B. Cohen, "Study of Supported Platinum Catalysts by Anomalous Scattering," *Journal of Catalysis*, vol. 92, no. 2, pp. 211–215, 1985.

[73] S. Nair, "Personal Communication.".

[74] K. Kim and N. Winograd, "X-ray Photoelectron Spectroscopic Binding Energy Shifts due to Matrix in Alloys and Small Supported Metal Particles," *Chemical Physics Letters*, vol. 30, no. 1, pp. 91–95, 1975.

[75] S. W. Gaarenstroom and N. Winograd, "Initial and Final State Effects in the ESCA Spectra of Cadmium and Silver Oxides," *Journal of Chemical Physics*, vol. 67, no. 10, pp. 3500–3506, 1977.

[76] G. Schön, "ESCA Studies of Ag, Ag_2O and AgO," *Acta Chemica Scandinavica*, vol. 27, pp. 2623–2633, 1973.

[77] J. S. Hammond, S. W. Gaarenstroom, and N. Winograd, "X-ray Photoelectron Spectroscopic Studies of Cadmium- and Silver-Oxygen Surfaces," *Analytical Chemistry*, vol. 47, no. 13, pp. 2193–2199, 1975.

[78] C. D. Wagner, L. E. Davis, M. V. Zeller, J. A. Taylor, R. H. Raymond, and L. H. Gale, "Empirical Atomic Sensitivity Factors for Quantitative Analysis by Electron Spectroscopy for Chemical Analysis," *Surface and Interface Analysis*, vol. 3, no. 5, pp. 211–225, 1981.

[79] C. D. Wagner, W. M. Riggs, L. E. Davis, J. F. Moulder, and G. E. Muilenberg, *Handbook of X-ray Photoelectron Spectroscopy.* Physical Electronics Division. Perkin-Elmer Corp., 1978.

[80] J. M. Heinsel, *Identification of Adsorption Mechanisms of Sulfur Heterocycles via Surface Analysis of Selected Metal-Doped Adsorbent Materials for Logistics Fuels Desulfurization.* PhD thesis, Auburn University, 2013.

[81] F. P. J. M. Kerkhof and J. A. Moulijn, "Quantitative Analysis of XPS Intensities for Supported Catalysts," *The Journal of Physical Chemistry*, vol. 83, no. 12, pp. 1612–1619, 1979.

[82] F. Delannay, C. Defosse, B. Delmon, P. G. Menon, and G. F. Froment, "Chloriding of $Pt - Al_2O_3$ Catalysts. Studies by Transmission Electron Microscopy and X-ray Photoelectron Spectroscopy," *Industrial & Engineering Chemistry Product Research and Development*, vol. 19, no. 4, pp. 537–541, 1980.

[83] H. P. C. E. Kuipers, H. C. E. Van Leuven, and W. M. Visser, "The Characterization of Heterogeneous Catalysts by XPS based on Geometrical Probability. 1: Monometallic Catalysts," *Surface and Interface Analysis*, vol. 8, no. 6, pp. 235–242, 1986.

[84] A. Meijers, A. de Jong, L. van Gruijthuijsen, and J. Niemantsverdriet, "Preparation of Zirconium Oxide on Silica and Characterization by X-ray Photoelectron Spectroscopy, Secondary Ion Mass Spectrometry, Temperature Programmed Oxidation and Infra-red Spectroscopy," *Applied Catalysis*, vol. 70, no. 1, pp. 53–71, 1991.

[85] P. W. Park and J. S. Ledford, "Characterization and CH_4 Oxidation Activity of Cr/Al_2O_3 Catalysts," *Langmuir*, vol. 13, no. 10, pp. 2726–2730, 1997.

[86] G. C. Smith, *Surface Analysis by Electron Spectroscopy: Measurement and Interpretation (Updates in Applied Physics and Electrical Technology)*. Springer, 1994.

[87] P. O. Scokart, A. Amin, C. Defosse, and P. G. Rouxhet, "Direct Probing of the Surface Properties of Alkali-Treated Aluminas by Infrared and X-ray Photoelectron Spectroscopy," *The Journal of Physical Chemistry*, vol. 85, no. 10, pp. 1406–1412, 1981.

[88] D. R. Penn, "Quantitative Chemical Analysis by ESCA," *Journal of Electron Spectroscopy and Related Phenomena*, vol. 9, no. 1, pp. 29–40, 1976.

[89] D. Briggs and M. P. Seah, eds., *Practical Surface Analysis: by Auger and X-ray Photoelectron Spectroscopy*. Chichester: Wiley, 1983.

[90] G. Wertheim, "New Method for Bulk Quantitative Analysis by ESCA," *Journal of Electron Spectroscopy and Related Phenomena*, vol. 50, no. 1, pp. 31–38, 1990.

[91] C. Battistoni, G. Mattogno, and E. Paparazzo, "Quantitative Surface Analysis by XPS: A Comparison among Different Quantitative Approaches," *Surface and Interface Analysis*, vol. 7, no. 3, pp. 117–121, 1985.

[92] S. Kumar, J. V. Ramana, V. S. Raju, J. Arunachalam, and S. Gangadharan, "Determination of Stoichiometry of Cadmium Telluride by XPS," *Fresenius' Journal of Analytical Chemistry*, vol. 343, pp. 879–880, 1992.

[93] D. Hayward and B. Trapnell, *Chemisorption*. Butterworth and Co. Ltd, 2nd ed., 1964.

[94] G. Wedler, *Chemisorption: An Experimental Approach*. Butterworth and Co. Ltd, 1970.

[95] I. E. Wachs, ed., *Characterization of Catalytic Materials*. Butterworth-Heinemann, 1992.

[96] W. W. Smeltzer, E. L. Tollefson, and A. Cambron, "Adsorption of Oxygen by a Silver Catalyst," *Canadian Journal of Chemistry*, vol. 34, no. 8, pp. 1046–1060, 1956.

[97] X. E. Verykios, F. P. Stein, and R. W. Coughlin, "Influence of Metal Crystallite Size and Morphology on Selectivity and Activity of Ethylene Oxidation Catalyzed by Supported Silver," *Journal of Catalysis*, vol. 66, no. 2, pp. 368–382, 1980.

[98] J. A. Weil, J. R. Bolton, and J. E. Wertz, *Electron Paramagnetic Resonance : Elementary Theory and Practical Applications*. John Wiley & Sons, Inc, 1994.

[99] S. J. Tauster, S. C. Fung, R. T. K. Baker, and J. A. Horsley, "Strong Interactions in Supported-Metal Catalysts," *Science*, vol. 211, pp. 1121–1125, 1981.

[100] S. J. Tauster, "Strong Metal-Support Interactions," *Accounts of Chemical Research*, vol. 20, no. 11, pp. 389–394, 1987.

[101] S. J. Tauster, S. C. Fung, and R. L. Garten, "Strong Metal-Support Interactions. Group 8 Noble Metals Supported onTitanium Dioxide," *Journal of the American Chemical Society*, vol. 100, no. 1, pp. 170–175, 1978.

[102] R. Baker, "Electron Microscopy Studies of Strong Metal-Support Interactions," in *Metal-Support and Metal-Additive Effects in Catalysis Proceedings of an International Symposium organized by the Institut de Recherches sur la Catalyse CNRS Villeurbanne and sponsored by the Centre National de la Recherche Scientifique* (B. Imelik, C. Naccache, G. Coudurier, H. Praliaud, P. Meriaudeau, P. Gallezot, G. Martin, and

J. Vedrine, eds.), vol. 11 of *Studies in Surface Science and Catalysis*, pp. 37 – 42, Elsevier, 1982.

[103] S. Kagawa, M. Iwamoto, S. Morita, and T. Seiyama, "Isotopic Study of the Temperature-Programmed Desorption of Oxygen from Silver," *J. Chem. Soc., Faraday Trans. 1*, vol. 78, pp. 143–146, 1982.

[104] T. Hoost, R. Kudla, K. Collins, and M. Chattha, "Characterization of Ag/γ-Al_2O_3 catalysts and their lean-NOx properties," *Applied Catalysis B: Environmental*, vol. 13, no. 1, pp. 59 – 67, 1997.

[105] K. L. Yeung, A. Gavriilidis, A. Varma, and M. M. Bhasin, "Effects of 1,2 Dichloroethane Addition on the Optimal Silver Catalyst Distribution in Pellets for Epoxidation of Ethylene," *Journal of Catalysis*, vol. 174, no. 1, pp. 1 – 12, 1998.

[106] K. Arve, K. Svennerberg, F. Klingstedt, K. Eränen, L. R. Wallenberg, J.-O. Bovin, L. Čapek, and D. Y. Murzin, "Structure-Activity Relationship in HC-SCR of NOx by TEM, O_2-Chemisorption, and EDXS Study of Ag/Al_2O_3," *The Journal of Physical Chemistry B*, vol. 110, no. 1, pp. 420–427, 2006. PMID: 16471551.

[107] JabRef Development Team, *JabRef*. JabRef Development Team, 2010.

[108] A. S. Hussain and B. J. Tatarchuk, "Adsorptive Desulfurization of Jet and Diesel Fuels using Ag/TiO_x-Al_2O_3 and Ag/TiO_x-SiO_2 Adsorbents," *Fuel*, vol. 107, pp. 465 – 473, 2013.

[109] A. S. Hussain and B. J. Tatarchuk, "Mechanism of Hydrocarbon Fuel Desulfurization using Ag/TiO_2–Al_2O_3 Adsorbent," *Fuel Processing Technology*, vol. 126, pp. 233 – 242, 2014.

[110] A. S. Hussain, M. L. Mckee, J. M. Heinzel, X. Sun, and B. J. Tatarchuk, "Density functional theory study of organosulfur selective adsorption on Ag/TiO_2 adsorbents," *The Journal of Physical Chemistry C*, vol. 118, no. 27, pp. 14938–14947, 2014.

[111] M. Lazzeri, A. Vittadini, and A. Selloni, "Structure and Energetics of Stoichiometric TiO_2 Anatase Surfaces," *Phys. Rev. B*, vol. 63, p. 155409, 2001.

[112] M. Lazzeri, A. Vittadini, and A. Selloni, "Erratum: Structure and energetics of stoichiometric TiO_2 anatase surfaces," *Phys. Rev. B*, vol. 65, p. 119901, 2002.

[113] C. L. Olson, J. Nelson, and M. S. Islam, "Defect Chemistry, Surface Structures, and Lithium Insertion in Anatase TiO_2," *The Journal of Physical Chemistry B*, vol. 110, no. 20, pp. 9995–10001, 2006.

[114] S.-C. Li, O. Dulub, and U. Diebold, "Scanning Tunneling Microscopy Study of a Vicinal Anatase TiO_2 Surface," *The Journal of Physical Chemistry C*, vol. 112, no. 42, pp. 16166–16170, 2008.

[115] U. Diebold, "The Surface Science of Titanium Dioxide," *Surface Science Reports*, vol. 48, no. 58, pp. 53 – 229, 2003.

[116] Y.-W. Jun, M. F. Casula, J.-H. Sim, S. Y. Kim, J. Cheon, and A. P. Alivisatos, "Surfactant-Assisted Elimination of a High Energy Facet as a Means of Controlling the Shapes of TiO_2 Nanocrystals," *Journal of the American Chemical Society*, vol. 125, no. 51, pp. 15981–15985, 2003.

[117] A. West, *Solid State Chemistry and Its Applications*. Wiley, 1987.

[118] S. Nair, A. S. Hussain, and B. J. Tatarchuk, "The Role of Surface Acidity in Adsorption of Aromatic Sulfur Heterocycles from Fuels," *Fuel*, vol. 105, pp. 695 – 704, 2013.

[119] S. Nair, H. Yang, and B. Tatarchuk, "Selectivity and Reactivity of Ag Based Adsorbents During Desulfurization of Logistic Fuels," AIChE Annual Meeting, 2007.

[120] S. Nair, H. Yang, and B. Tatarchuk, "Advanced Adsorbents for Ultra Deep Desulfurization of Logistic Fuels Using Micro-Fiber Entrapped Particles," AIChE Annual Meeting, 2007.

[121] S. Nair, *Desulfurization of Hydrocarbon Fuels at Ambient Conditions Using Supported Silver Oxide-Titania Sorbents.* PhD thesis, Auburn University, 2010.

[122] A. S. Hussain, *Liquid Phase Desulfurization of Hydrocarbon Fuels under Ambient Conditions using Regenerable Mixed Oxide Supported Silver Adsorbents.* PhD thesis, Auburn University, 2014.

[123] J. M. Heinzel, *Identification of Adsorption Mechanisms of Sulfur Heterocycles via Surface Analysis of Selected Metal-Doped Adsorbent Materials for Logistics Fuels Desulfurization.* PhD thesis, Auburn University, 2013.

[124] Z. Davis, "Laboratory notebook." 2012.

[125] H. G. Karge and V. Dondur, "Investigation of the Distribution of Acidity in Zeolites by Temperature-Programmed Desorption of Probe Molecules. I. Dealuminated Mordenites," *The Journal of Physical Chemistry*, vol. 94, no. 2, pp. 765–772, 1990.

[126] C. U. I. Odenbrand, J. G. M. Brandin, and G. Busca, "Surface Acidity of Silica-Titania Mixed Oxides.," *ChemInform*, vol. 23, no. 36, pp. no–no, 1992.

[127] A. Auroux, R. Monaci, E. Rombi, V. Solinas, A. Sorrentino, and E. Santacesaria, "Acid Sites Investigation of Simple and Mixed Cxides by TPD and Microcalorimetric techniques," *Thermochimica Acta*, vol. 379, no. 1-2, pp. 227 – 231, 2001.

[128] F. Arena, R. Dario, and A. Parmaliana, "A Characterization Study of the Surface Acidity of Solid Catalysts by Temperature Programmed Methods," *Applied Catalysis A: General*, vol. 170, no. 1, pp. 127 – 137, 1998.

[129] P. A. Thiel, M. Shen, D.-J. Liu, and J. W. Evans, "Adsorbate-Enhanced Transport of Metals on Metal Surfaces: Oxygen and Sulfur on Coinage Metals," *Journal of Vacuum Science & Technology A: Vacuum, Surfaces, and Films*, vol. 28, no. 6, pp. 1285–1298, 2010.

[130] M. Shen, C. Jenks, J. Evans, and P. Thiel, "How Sulfur Controls Nucleation of Ag Islands on Ag(111)," *Topics in Catalysis*, vol. 54, pp. 83–89, 2011.

[131] M. Danilczuk, A. Lund, J. Sadlo, H. Yamada, and J. Michalik, "Conduction Electron Spin Resonance of Small Silver Particles," *Spectrochimica Acta Part A: Molecular and Biomolecular Spectroscopy*, vol. 63, no. 1, pp. 189–191, 2006.

[132] S. Livraghi, M. Paganini, M. Chiesa, and E. Giamello, "Trapped Molecular Species in N-doped TiO_2," *Research on Chemical Intermediates*, vol. 33, pp. 739–747, 2007.

[133] P. G. Baranov, R. A. Zhitnikov, and N. I. Melnikov, "Paramagnetic Resonance of Silver Atoms Stabilized in Alkali Halide Crystals," *Physica Status Solidi (b)*, vol. 30, no. 2, pp. 851–858, 1968.

[134] B. Bales and L. Kevan, "EPR of Ag^0 Site Conversion in Gamma-irradiated Frozen $AgNO_3$ Ices," *Chemical Physics Letters*, vol. 3, no. 7, pp. 484–487, 1969.

[135] G. E. Holmberg, W. P. Unruh, and R. J. Friauf, "An ESR and ENDOR Study of the Ag^0 Center in KCl and NaCl," *Phys. Rev. B*, vol. 13, pp. 983–992, 1976.

[136] Y.-P. Wang and C.-T. Yeh, "Electron Paramagnetic Resonance Study of the Interactions of Oxygen with Silver/Titania," *Journal of the Chemical Society, Faraday Transactions*, vol. 87, pp. 345–348, 1991.

[137] R. Borade, A. Sayari, A. Adnot, and S. Kaliaguine, "Characterization of Acidity in ZSM-5 Zeolites: An X-ray Photoelectron and IR Spectroscopy Study," *The Journal of Physical Chemistry*, vol. 94, no. 15, pp. 5989–5994, 1990.

[138] C. Defossé, P. Canesson, P. Rouxhet, and B. Delmon, "Surface Characterization of Silica-Aluminas by Photoelectron Spectroscopy," *Journal of Catalysis*, vol. 51, no. 2, pp. 269–277, 1977.

[139] G. Somorjai and Y. Li, *Introduction to Surface Chemistry and Catalysis*. John Wiley & Sons Limited, 2nd ed., 2010.

[140] R. J. Culbertson, L. C. Feldman, P. J. Silverman, and H. Boehm, "Epitaxy of Au on Ag(111) Studied by High-Energy Ion Scattering," *Phys. Rev. Lett.*, vol. 47, pp. 657–660, 1981.

[141] D. R. Lide, ed., *CRC Handbook of Chemistry and Physics*. CRC Press, 86 ed., 2005.

[142] J. H. Scofield, "Hartree-Slater Subshell Photoionization Cross-sections at 1254 and 1487 eV," *Journal of Electron Spectroscopy and Related Phenomena*, vol. 8, no. 2, pp. 129–137, 1976.

Appendices

Appendix A

Physical Properties

Useful Silver Properties

Ag metallic radius	1.45	Å
Ag^{1+} ionic radius	1.26	Å
Ag^{2+} ionic radius	1.01	Å
Ag atomic weight	107.867	g/mol
Ag density	1.05×10^{7}	g/m^3
Ag density	10.50	g/cc
Ag NN interatomic distance	2.889	Å
Ag(111) fcc surface spacing [139, 140]	2.35 ± 0.1	Å
Ag(110) fcc surface spacing [139]	1.33 ± 0.04	Å
Ag fcc lattice parameter [141]	4.08	Å
Ag active surface atom cross-sectional area [22]	8.6960	$Å^2$/Ag atom
Ag photoemission cross-section Ag $3d_{5/2}$ Al-Kα [142]	1.45×10^{-23}	m^2
	10.66	13600 barns
Ag photoemission cross-section Ag $3d_{3/2}$ Al-Kα [142]	1.00×10^{-23}	m^2
	7.38	13600 barns
Ag photoemission cross-section Ag $3d_{5/2}$ Mg-Kα [142]	2.37×10^{-23}	m^2
Mean free path (1118 eV) Ag $3d_{5/2}$ Al-Kα, λ [88]	1.38×10^{-9}	m

Useful Titanium Properties

TiO_2 molecular weight	79.9	g/mol
Ti density	4.23×10^{6}	g/m^3
Ti density	4.23	g/cc
Ti photoemission cross-section Ti $2p_{1/2}$ Al-Kα [142]	3.66×10^{-24}	m^2
	2.69	13600 barns
Ti photoemission cross-section Ti $2p_{3/2}$ Al-Kα [142]	7.10×10^{-24}	m^2
	5.22	13600 barns
Mean free path (1118 eV) Ti $2p_{1/2}$ Al-Kα, λ [88]	1.62×10^{-9}	m

Other Useful Properties		
Al-Kα line width [89]	0.85	eV
Al-Kα line x-ray energy	1486.6	eV
Mg-Kα x-ray energy	1253.6	eV
Mg-Kα line width[89]	0.70	eV
Bohr radius,a_0,	0.529	Å

Appendix B

Supplemental Information

B.1 Oxygen Chemisorption Treatment Sequence

1. Change gas input to hydrogen
2. Set furnace to 150°C at 30 °C/min
3. Evacuate until setpoint
4. Evacuate for 30 minutes
5. Set furnace to 400 °C at 10 °C/min
6. Evacuate until setpoint
7. Flow for 60 minutes
8. Evacuate for 60 minutes
9. Set furnace to 170°C at 10°C/min
10. Evacuate until setpoint
11. Change gas input to oxygen

B.2 Temperature Programmed Reduction Treatment Sequence

1. Change gas input to air flowing at approximately 90 ml/min
2. Set furnace to 115 °C at 30 °C/min
3. Evacuate until setpoint
4. Flow air for 15-20 minutes at 115 °C to remove water vapour
5. Cool to room temperature
6. Change gas input to argon at 15 ml/min for inert air pretreatment
7. Flow for 30-45 mintues
8. Place cold trap before TCD stream to remove water form exit stream
9. Change gas input to rectant gas, 5% H_2/Ar
10. Flush lines for 30 minutes
11. Heat sample from 30 °C to 650 °C at 10 °C/min
12. Change gas input to argon

Percent Site	Percent Max Atomic Growth		
Increase	8 wt%	12 wt%	20 wt%
0	25.10	15.52	11.83
10	20.56	15.42	11.83
20	16.76	11.57	9.37
30	13.55	10.08	8.42
40	10.79	8.82	7.61
50	8.41	7.71	6.91
60	6.32	6.72	6.29
70	4.48	5.90	5.75
80	2.82	5.14	5.27
90	1.37	4.47	4.83
100	0.06	3.86	4.44

Table B.1: Fraction of Base Sites on TiO_2 Occupied by Ag Agglomerates (see Figure 6.3 for corresponding graph)

Appendix C

TPR Supplemental Information

```
%matplotlib inline
import numpy as np
import os
from pylab import \*

#cd ~/tmp/Zenda/TPR_Numerical_Integration
path = r'\Users\daviszd\Desktop\tprplotdata\TPRData'
os.chdir(path)
os.listdir(path)

class TPR():
    def __init__(self, filename):
        # read the text of the file into the variable read_data
        with open(filename, 'r') as f:
            read_data = f.read()
        # split the raw text into lines
        self.data = read_data.split('\n')[1:]
        self.filename = filename

        # set up empty vectors to hold the data from the file
        temperature = []
        au = []
        # store the first value in each line (index 0) in the temperature vector
```

```
    # and the second value in each line (index 1) in the au vector
    for line in self.data:
        if line == '': continue
        else:
            # print(line)
            splitline = line.split()
            temperature.append(float(splitline[0]))
            au.append(float(splitline[1]))
    # Adjust the au values to be positive
    minau = min(au)
    self.rawau = au
    au = [y - minau for y in au]
    self.au = au
    self.temperature = temperature

def plot(self):
    figure()
    plot(self.temperature, self.au)
    xlabel('Temperature')
    ylabel('au')
    show()



def integrate(self, xmin, xmax):
    x = self.temperature
    y = self.au
    start_index = 0
```

```
        stop_index = -1
        for i,v in enumerate(x):
            if v < xmin: start_index = i
            if v < xmax: stop_index= i
        print('index: {} - {}'.format(start_index,stop_index))
        print('temp: {} - {}'.format(x[start_index], x[stop_index]))
        print('au: {} - {}'.format(y[start_index], y[stop_index]))
        xdata = x[start_index:stop_index]
        ydata = y[start_index:stop_index]
        miny = min(ydata)
        ydata_adjusted = [i + abs(miny) for i in ydata]
        integral = np.trapz(ydata_adjusted, xdata)
        print('integral: {}'.format(integral))
        self.integral = integral
        return(integral)


filename = os.path.join(path, '6wt-2.txt')
test = TPR(filename)
test.integrate(130,250)
#test1.plot()

# Example function calls
# manually edit the secondary peak search region
# This is the x-coordinate of the vertical line that separates the first two peaks
# It needs to intersect the line in the valley between the first two peaks
# i.e. separation=# Temperature in the valley
isolate_peaks(test.temperature, test.au, xmin=90, xmax=500, separation_temp=215,
```

```
Temperature_offset=0)
```